



## OPEN ACCESS

## EDITED BY

Germana Garofalo,  
Istituto per le Risorse Biologiche e le  
Biotecnologie Marine del Consiglio  
Nazionale delle Ricerche (IRBIM CNR),  
Italy

## REVIEWED BY

Bernardo Patti,  
National Research Council (CNR), Italy  
Alejandro Gallego,  
Marine Scotland, United Kingdom

## \*CORRESPONDENCE

Costanza Cappelli  
✉ [cosca@aqu.dtu.dk](mailto:cosca@aqu.dtu.dk)

RECEIVED 15 January 2026

REVISED 22 February 2026

ACCEPTED 24 February 2026

PUBLISHED 13 March 2026

## CITATION

Cappelli C, Hátún H, Jacobsen JA,  
Visser AW, Hansen FT, Mortensen JB,  
Accornero S, Rodrigues F and  
MacKenzie BR (2026) Circulation-driven  
dispersal and retention affect blue  
whiting recruitment dynamics in the  
Northeast Atlantic Ocean.  
*Front. Mar. Sci.* 13:1764145.  
doi: 10.3389/fmars.2026.1764145

## COPYRIGHT

© 2026 Cappelli, Hátún, Jacobsen, Visser,  
Hansen, Mortensen, Accornero, Rodrigues  
and MacKenzie. This is an open-access  
article distributed under the terms of the  
[Creative Commons Attribution License  
\(CC BY\)](https://creativecommons.org/licenses/by/4.0/). The use, distribution or  
reproduction in other forums is  
permitted, provided the original  
author(s) and the copyright owner(s) are  
credited and that the original publication  
in this journal is cited, in accordance  
with accepted academic practice. No  
use, distribution or reproduction is  
permitted which does not comply with  
these terms.

# Circulation-driven dispersal and retention affect blue whiting recruitment dynamics in the Northeast Atlantic Ocean

Costanza Cappelli<sup>1\*</sup>, Hjalmar Hátún<sup>2</sup>, Jan Arge Jacobsen<sup>2</sup>,  
André W. Visser<sup>1</sup>, Flemming Thorbjørn Hansen<sup>3</sup>,  
Jonas B. Mortensen<sup>3</sup>, Sara Accornero<sup>3</sup>, Francisca Rodrigues<sup>1</sup>  
and Brian R. MacKenzie<sup>1</sup>

<sup>1</sup>Section for Oceans and Arctic, National Institute of Aquatic Resources (Technical University of Denmark (DTU) Aqua), Lyngby, Denmark, <sup>2</sup>Faroe Marine Research Institute, Tórshavn, Faroe Islands, <sup>3</sup>Danish Hydraulic Institute (DHI) A/S, Hørsholm, Denmark

Environmental drivers of early life-stage survival are critical to understanding recruitment variability and improving ecosystem-based fisheries management. We investigate how regional ocean circulation influences blue whiting (*Micromesistius poutassou*) recruitment in the Northeast Atlantic by combining multi-decadal transport analyses with Lagrangian particle simulations. Using ocean reanalysis, we compute 28-year (1993–2020) volume transport indices across the Ellett Line, a hydrographic section through the main spawning grounds, and we relate them to interannual variation in recruit per spawner. We also simulate larval dispersal from main spawning areas (Porcupine Bank, Rockall Trough, Rockall Plateau, Hebrides) during the six highest and lowest recruit-per-spawner years using an agent-based particle-tracking model. Statistical models show that higher recruit per spawners are produced in years with stronger northward flow along the Hebrides-Rockall Trough (upper 0–100 m), whereas transport over Rockall Plateau is weaker and exhibits no consistent relationship with recruit per spawner. Complementary particle-tracking simulations reveal that high-recruit-per-spawner years are characterized by larger northward advection of eggs and larvae from the Hebrides, as well as increased local retention over Porcupine Bank. In contrast, low-recruit-per-spawner years exhibit more meandering drift in the Rockall region and a modest southward dispersal from Porcupine Bank. These results suggest that both effective transport to known northern nursery areas and retention in productive spawning regions can enhance early survival, depending on spawning location. We propose that large-scale ocean-climate variability (e.g., changes in subpolar gyre circulation driven by wind stress curl) modulates these transport mechanisms, thereby influencing whether early life stages are delivered to favorable habitats or lost to suboptimal areas. Our findings provide a mechanistic link between climate-driven circulation changes and fish recruitment variability, underscoring a potential benefit of incorporating oceanographic processes into ecosystem-based fisheries management strategies.

## KEYWORDS

agent-based model, blue whiting, egg and larval dispersal, recruitment variability, transport

# 1 Introduction

Understanding the environmental drivers of early stage survival of fishes is central to explaining population fluctuations and to strengthening the ecosystem basis for sustainable fisheries management (Roux and Pedreschi, 2024). Blue whiting (*Micromesistius poutassou*) is a small mesopelagic gadoid widely distributed across the Northeast Atlantic, from the European shelf and Porcupine Bank northward to the Norwegian and Barents Seas and west toward Iceland and Greenland (Pointin and Payne, 2014; Trenkel et al., 2014; Post et al., 2021; ICES, 2022, 2024). Its main spawning grounds are concentrated along the continental shelf break west of Ireland and the British Isles, especially around Porcupine Bank, Rockall Trough, Rockall Plateau and west of the Hebrides (Figure 1), while the main nursery areas lie along the continental shelf break, in the Norwegian Sea and toward the southern Icelandic shelf (Trenkel et al., 2014; Miesner et al., 2022; ICES, 2022, 2024). Ecologically, blue whiting occupies a mid-trophic position as an abundant zooplanktivore that can locally affect the abundance of preferred prey species, and can itself be a major prey item for higher predators (Hátún et al., 2009a; Bachiller et al., 2016; Post et al., 2021). Commercially, the stock supports one of the largest pelagic fisheries in the North Atlantic and remains a key resource for local economies across the region (ICES, 2022, 2024). Despite its ecological and commercial importance, the environmental processes affecting blue whiting population productivity metrics, including recruitment, remain poorly understood. This knowledge gap adds uncertainty to forecasts of future stock dynamics and to sustainable, ecosystem-based management (ICES, 2024).

Recent work indicates that ocean-climate conditions in the Northeast Atlantic influence blue whiting recruitment success.

For example, Cappelli et al. (2025) show that survival during the early stages covaries with wind-stress curl (WSC), an atmospheric driver of the regional circulation, and Laiz et al. (2025) show that retention processes near one of the spawning areas can affect survival.

Interannual changes in WSC in the Northeast Atlantic alter pathways of currents, frontal positions, and water-mass distributions around blue whiting main spawning grounds (Holliday, 2003; Häkkinen et al., 2011; Hátún et al., 2021). Through Sverdrup dynamics, WSC strengthens/weakens and shifts the North Atlantic subpolar gyre (SPG), modulating exchanges between subtropical and subpolar waters and the position and strength of North Atlantic Current (NAC) branches that feed the upper limb of the Atlantic Meridional Overturning Circulation (AMOC) (Eden and Willebrand, 2001; Häkkinen and Rhines, 2004; Hátún et al., 2005; Chafik et al., 2019). SPG variability steers the NAC toward or away from the northwest European shelf break, thereby regulating the inflow across the Rockall region that hosts the main blue whiting spawning grounds (Hátún et al., 2009a, 2009b; Lee et al., 2025).

SPG variability has been associated with variability in the distribution of blue whiting spawners at spawning time (Hátún et al., 2009b) and of young blue whiting larvae (Miesner and Payne, 2018). When the SPG is weak and contracted, relatively warm, saline subtropical waters penetrate farther north along the European slope and westward across Rockall Plateau. Consequently, spawning extends northward and westward and tends to occur in saltier ( $\geq 35.35$ ) and warmer ( $\geq 10^\circ\text{C}$ ) layers that can potentially favor larval growth and reduce predation risk (Hátún et al., 2009b; Payne et al., 2012; Miesner and Payne, 2018). Conversely, during a strong and expanded SPG, cooler, fresher subpolar waters dominate, confining high salinities to the Hebrides slope and in a southerly position near Porcupine Bank, limiting the

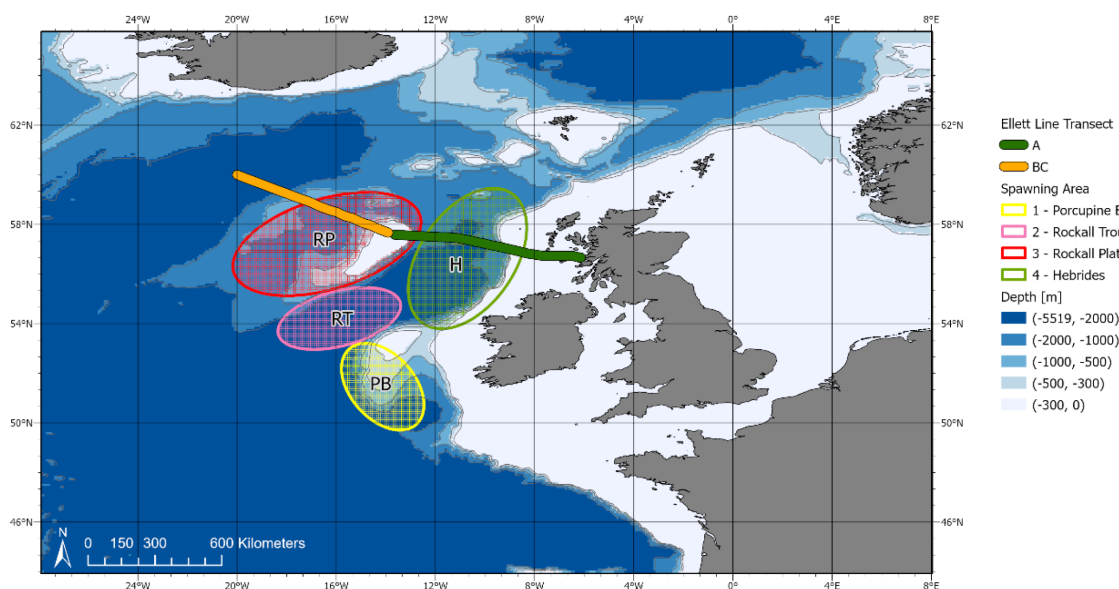


FIGURE 1

Map of the Northeast Atlantic showing the Ellett Line transects (A, BC) and the four blue whiting spawning areas used in the agent-based model (ABM) simulations (Porcupine Bank, Rockall Trough, Rockall Plateau, and Hebrides) overlaid on bathymetry. The map delineates the ABM spatial domain (30° W-8° E, 44-66° N).

spatial extent of spawning to these areas (Hátún et al., 2009b; Miesner and Payne, 2018). Such shifts in spawning location may expose eggs and larvae to different transport pathways with more or less favorable drift and retention conditions in different years, with consequences for early survival.

WSC affects blue whiting spawning habitat in additional ways. Via Ekman pumping, positive WSC drives surface divergence and upwelling, that can enhance nutrient supply and lower-trophic productivity (Hátún et al., 2021), potentially improving feeding conditions for larvae (Williams and Follows, 2003; Jacox et al., 2018). WSC also drives interannual changes in vertical mixing and subduction (Hátún et al., 2021), that ventilate the permanent thermocline (van Aken, 2001), thereby modifying temperature-salinity fields encountered by eggs and larvae. Such shifts can influence physiological rates; for example, blue whiting egg hatch success declines sharply above  $\sim 10\text{--}12^\circ\text{C}$  (Coombs and Hiby, 1979; Bailey and Heath, 2001).

The long-term mean WSC zero-line (WSC = 0), which in an idealized ocean separates the subtropical and subpolar gyres, crosses the Rockall region (Cappelli et al., 2025). Its year-to-year meridional shifts overlap the largest known blue whiting spawning grounds, implying interannual changes in advection and vertical mixing over the spawning habitat (Cappelli et al., 2025). As a result, eggs and larvae may experience different transport pathways from spawning to nursery areas in different years. Depending on wind stress conditions, eggs and larvae released along the shelf break may be exported northward in some years, retained locally, or advected southward in others. High-WSC states can potentially enhance dispersal toward northern nurseries (e.g., Faroes, the shelf south of Iceland and East Greenland, the Norwegian Sea and Norwegian coast), whereas other wind regimes favor retention or southward transport toward the Celtic Sea and Bay of Biscay (Bartsch and Coombs, 1997; Eden and Willebrand, 2001; Kloppmann et al., 2001; Brophy and King, 2007; Was et al., 2008). Recent observational analyses show that anomalously low wind mixing in 2020 produced a Taylor column over Porcupine Bank, greatly increasing local retention and contributing to the extraordinary blue whiting recruitment in that year (Laiz et al., 2025). However, the exact causal links from WSC to blue whiting recruitment remain uncertain.

Numerous studies have demonstrated that interannual variability in circulation patterns, such as prevailing currents and retention zones, can strongly affect egg and larval drift pathways from spawning to nursery areas and, ultimately, drive recruitment success (e.g., Henriksen et al., 2018; Romagnoni et al., 2020). Changes in transport and mixing can affect the exposure of eggs and larvae to biotic (prey availability, predation) and abiotic (temperature, salinity, nutrients) conditions during sensitive early life stages (Sinclair, 1988; Bartsch and Coombs, 1997; Ådlandsvik et al., 2001; Hátún et al., 2021). This linkage is increasingly quantified by biophysical agent-based models that relate current-driven dispersal, growth conditions, and survival of early life stages to subsequent recruitment (e.g., Romagnoni et al., 2020; Jansen et al., 2021; Pereira Gabellini et al., 2023).

Here we test the role of regional circulation and transport on the survival of blue whiting early life history stages by combining two

complementary approaches. First, we estimate volume transport across the Ellett Line, a long-running monitoring section that crosses blue whiting main spawning grounds west of the British Isles, and we use the derived flow indices in statistical models to assess their relationship with blue whiting recruit per spawner over the 28 years (1993–2020) of available hydrographic data. Second, we build an agent-based model (ABM) to simulate egg and larval drift from the spawning areas, and we quantify dispersal and retention focusing on years of exceptionally high and low recruit per spawner. Together, these analyses allow us to evaluate whether interannual differences in transport processes during the first months post-spawning help explain the variability in blue whiting recruitment and place the WSC-recruitment link (Cappelli et al., 2025) into a mechanistic framework relevant to ecosystem-based fisheries management.

## 2 Materials and methods

### 2.1 Transport analyses

#### 2.1.1 Flow estimates: transects and areas analyzed, GLORYS velocity data, flow calculation

We analyze transport across the Extended Ellett Line (EEL, for simplicity EL), a hydrographic section comprising 69 stations from the Scottish shelf to Iceland and crosses the Hebrides, Rockall Trough, and Rockall Plateau (Supplementary Figure 1A). At each station, spaced at  $\sim 30$  km intervals, profiles of currents, temperature, salinity, and other water-column properties are collected from surface to seafloor, providing multi-decadal datasets in the eastern subpolar North Atlantic. The EL samples the northward inflow of warm, saline water in branches of the NAC (the upper limb of the AMOC) as well as returning dense overflows. Therefore, it is widely used to monitor variability linked to the SPG and AMOC in the region adjacent to the main blue whiting spawning grounds along the shelf break. For the flow analyses, we focus on two straight EL transects A and BC spanning the main blue whiting spawning grounds (Figure 1). Transect A extends from station 1G ( $56.67^\circ\text{N}$ ,  $6.13^\circ\text{W}$ ) to station A ( $57.58^\circ\text{N}$ ,  $13.63^\circ\text{W}$ ) across the Hebrides and Rockall Trough. Transect BC crosses Rockall Plateau and it combines transect B, which extends from IB1 ( $57.67^\circ\text{N}$ ,  $13.90^\circ\text{W}$ ) to IB4 ( $58.50^\circ\text{N}$ ,  $16.00^\circ\text{W}$ ), and transect C from IB4A ( $58.57^\circ\text{N}$ ,  $16.25^\circ\text{W}$ ) to IB12 ( $60.00^\circ\text{N}$ ,  $20.00^\circ\text{W}$ ) (Supplementary Figure 1B). We define transects by the angle of each line segment relative to the eastward (x) axis; a new transect begins where the orientation changes by  $>10^\circ$ , and each includes at least three stations. We treat BC as a single transect by summing transport computed separately for B and C. Station coordinates are obtained from the Extended Ellett Line portal (National Oceanography Centre, accessed 3 September 2024).

We estimate transport for 1993–2020 along transects A (1G-A) and BC (IB1-IB12) using monthly eastward (u) and northward (v) current velocities from the CMEMS Global Ocean Physics Reanalysis GLORYS12V1 (DOI: 10.48670/moi-00021; Lellouche et al., 2021), provided by the E.U. Copernicus Marine Service (Copernicus Marine Service, 2021). GLORYS12V1 employs a 1/

12° quasi-isotropic horizontal grid and 50 vertical levels with thickness increasing with depth. This high-resolution ocean reanalysis is corroborated by observations and other reanalyses and is considered to provide reliable estimates of current velocities and direction in the Nordic Seas, Faroe-Shetland Channel, and subpolar North Atlantic region (e.g., Verezhemskaya et al., 2021; Chafik et al., 2023; Huang et al., 2023; Ártun et al., 2025). The selected time period (1993–2020) covers the full time series of data available from Copernicus at the time of our study.

For each transect (A and BC), we build two regular grids (0–100 m and 0–400 m) with horizontal cell length  $\Delta x \sim 25$  km and vertical thickness  $\Delta z = 50$  m. GLORYS fields are filtered to a padded box around each transect ( $\pm 0.08^\circ$  in both latitude and longitude) and linearly interpolated to cell centers in (lat, lon, depth). The velocity normal to the transect is expressed as:

$$V_n = v \cos \theta + u \sin \theta$$

where  $\theta$  is the transect angle relative to the eastward (x) axis, computed from the end-point coordinates as the arctangent of the slope of the transect:

$$\theta = \arctan 2 (\Delta lat, \Delta lon)$$

The transport ( $Q$ ) through each grid cell is calculated as the product of the velocity and the cross-sectional area:

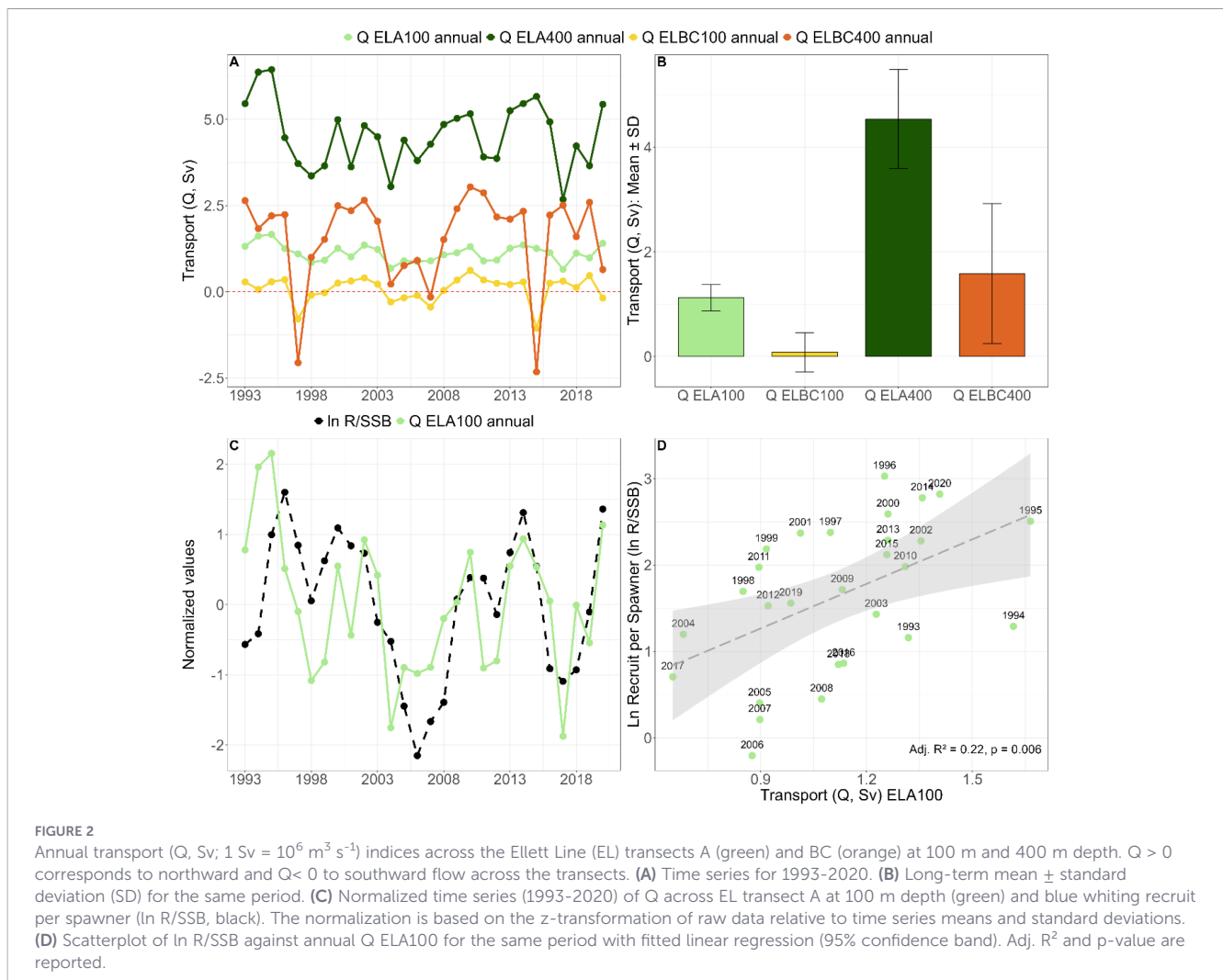
$$q_i = v_n \Delta x \Delta z$$

The total transport through the transect is the sum of the transport across each cell, given by:

$$Q = \sum q_i$$

Transport is expressed in Sverdrup ( $1 \text{ Sv} = 10^6 \text{ m}^3 \text{ s}^{-1}$ ). We define  $Q$  so that positive values indicate northward (poleward) transport across each transect, whereas negative values indicate southward flow.

From the monthly transports, we derive annual time series for 1993–2020 by averaging January–December values for EL transects A and BC, each integrated over 0–100 m and 0–400 m depth. Data from Copernicus beyond July 2021 were incomplete; therefore, 2021 was excluded from the transport analyses. This results in four time series of 28 years of annual transport ( $Q$ ) estimates: ELA100, ELA400, ELBC100, ELBC400 (Figure 2A, Supplementary Figure S2). For each series, we report the 1993–2020 mean and standard deviation (Figure 2B). We use the four annual transport indices as predictors in the statistical analyses, as described below.



We repeat the same analyses using transport indices computed over March-May for the same transects and depth ranges as the annual means, covering the peak blue-whiting spawning season (Hátún et al., 2009b; Miesner and Payne, 2018; Miesner et al., 2022; ICES, 2022, 2024). Flow estimates and statistical analyses based on the seasonal transport means are shown in the Supplementary Material (Supplementary Figure S3, S4; Supplementary Table 1).

### 2.1.2 Statistical analyses: data, models, model performance, model diagnostics

To assess the influence of transport across the EL on blue whiting early life history we obtain data on blue whiting recruitment (R) and spawning stock biomass (SSB) for the Northeast Atlantic (ICES Subareas 1-9, 12, 14) from the 2024 ICES stock assessment (ICES, 2024). Recruitment is reported as numbers of one-year-olds; therefore, R is shifted back one year to its birth year (yearclass). In this study, we use the natural logarithm of recruit per spawner ( $\ln R/SSB$ ) as response variable in the statistical models (Figures 2C, 3).

We use a 28-year time series (1993-2020, Supplementary Figure 2) of blue whiting  $\ln R/SSB$  and each of the four transport indices Q (ELA100, ELA400, ELBC100, ELBC400) to fit single-predictor linear regressions:

$$\ln\left(\frac{R}{SSB}\right) = \ln(a) + b * Q$$

For each transport index, we also fit an autoregressive model that uses Q as fixed-effect covariate and includes a first-order autoregressive (AR(1)) structure in the residuals to account for temporal dependence:

$$\ln\left(\frac{R}{SSB}\right) = \ln(a) + b * Q + \varepsilon_y$$

where  $\varepsilon_y = \rho * \varepsilon_{y-1} + \omega_y$  and  $\omega_y \sim N(0, \sigma^2)$ . Here,  $\varepsilon_y$  is the residual at time  $y$ ,  $\rho$  is the autoregressive parameter ( $|\rho| < 1$ ), and  $\omega_y$  is a white noise process.

In addition, we fit an autoregressive-only model (A1), where  $\ln R/SSB$  is modelled solely with an AR(1) residual structure and no transport covariate:

$$\ln\left(\frac{R_y}{SSB_y}\right) = \ln(a) + \varepsilon_y$$

where  $\varepsilon_y$  is the autocorrelation term as defined as above.

We also fit a geometric-mean  $\ln R/SSB$  model for 1993-2020 (GM; intercept only) as baseline model for comparison.

All models are fitted with the *glmmTMB* package (Brooks et al., 2017; Magnusson et al., 2019) in R 4.2.0 (R Core Team), assuming Gaussian residuals for  $\ln(R/SSB)$  (i.e.,  $\varepsilon_y \sim N(0, \sigma^2)$ ) and, where specified, an AR(1) residual correlation structure.

We compare goodness of fit using the small-sample-corrected Akaike Information Criterion (AICc) (Akaike, 1973; Burnham et al., 2011) and report each model's maximized log-likelihood ( $\log Lik$ ). We compute the Akaike difference relative to the baseline model (GM) as  $\Delta_i = AICc_{GM} - AICc_{model_i}$  so positive values indicate improvement over GM. Note that  $\Delta_i < 2$  is typically interpreted as indicating similar model performance (Burnham and Anderson, 2002). The corresponding evidence ratio is calculated as  $ER = \exp(\Delta_i/2)$ , thus  $ER > 1$  indicates greater support than GM. For overall ranking, the model with the smallest AICc is selected as the best among candidates to explain the variability in blue whiting recruit per spawner between 1993 and 2020.

To explore broader ocean-climate influences on transport, we also model each transport index (Q) as a function of the subpolar gyre (SPG) index (Hátún and Chafik, 2018) or wind stress curl (WSC) (Cappelli et al., 2025), using the same framework. Full

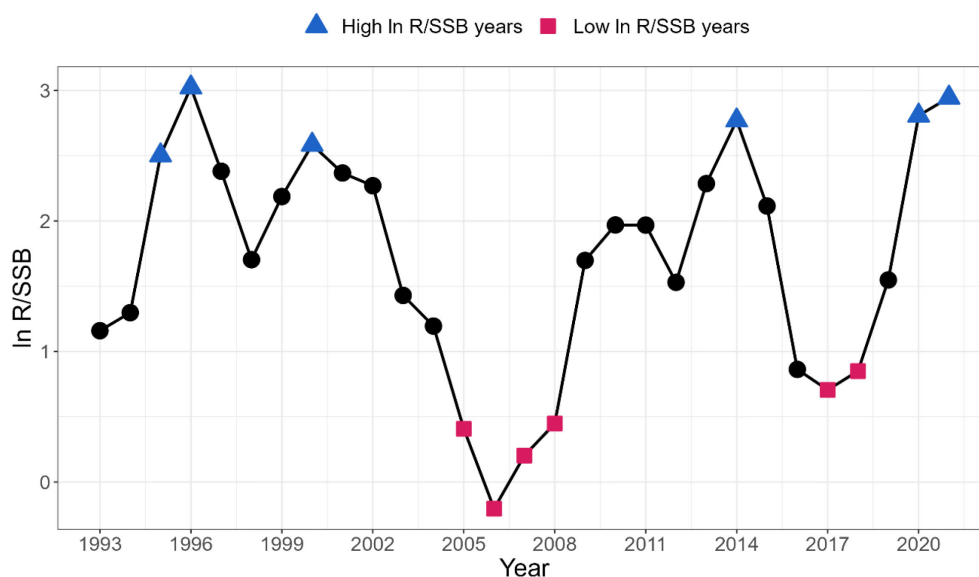


FIGURE 3

Time series of blue whiting recruit per spawner ( $\ln R/SSB$ ) (1993-2021). The six highest and lowest  $R/SSB$  years are shown with blue triangles and red squares, respectively, indicating the years selected for the ABM runs. Data for R (numbers of 1-year-olds, shifted back to birthyear) and SSB are sourced from the 2024 report by the ICES Working Group on Widely Distributed Stocks (WGWIDE) (ICES 2024).

specifications and results for the Q-SPG/WSC analyses are provided in the Supplementary Material (SPG: [Supplementary Figure 5](#); [Supplementary Table 2](#); WSC: [Supplementary Figures 6–S7](#)).

For each model fitted, we conduct diagnostic analyses (check for normality, time trends, biases, and autocorrelation) on the one-step ahead prediction errors using a rolling time series cross-validation (Thygesen et al., 2017; Bergmeir et al., 2018). Details and plots are presented in the Supplementary Material ([Supplementary Figures 8–S13](#)).

In addition, we extract current velocity from 1993–2020 (annual averages, January–December; and spawning-season averages, March–May) through the EL (A, B, C) from the surface to 1500 m ([Supplementary Figure 14](#), [S15](#)). At each depth-longitude position, we correlate these current velocities with (i)  $\ln R/SSB$ , (ii) the SPG index, and (iii) the WSC index. Results are shown in the Supplementary Material ([Supplementary Figure 16–S17](#)).

All statistical analyses are performed in RStudio using R 4.2.0 (R Core Team), and spatial maps are generated in ArcGIS Pro 3.0.0 (Esri, Redlands, CA, USA) (Esri, ArcGIS pro (version 3.0.0), 2022).

## 2.2 Agent-based model analyses

### 2.2.1 Software and oceanographic data

We simulate the dispersal of blue whiting larvae using ABM Lab (DHI, 2016a), an agent-based particle-tracking model, coupled to a 3D hydrodynamic ocean circulation system (MIKE 3 FM; DHI, 2016b). Simulations are forced with daily GLORYS12V1 reanalysis fields of eastward and northward currents ( $u$ ,  $v$ ) for the selected ABM years. In our study domain (30° W–8° E, 44–66° N; [Figure 1](#)), the grid spacing is ~9.3 km in latitude and ~6.7 km (44° N) to 3.8 km (66° N) in longitude. Data are extracted to cover the horizontal extent of the study area ([Figure 1](#)) and down to a maximum water depth of ~550 m. Prior to the ABM setup, the GLORYS fields are converted from NetCDF (.nc) to MIKE data format (\*.dfsu) and re-gridded vertically by linear interpolation every 10 m from the surface to ~541 m, resulting in 54 uniform layers (deeper levels are not used). The converted GLORYS data are applied as a forcing to the ABM Lab configuration.

### 2.2.2 ABM formulation

We formulate an ABM to track the dispersal of particles representing blue whiting eggs and larvae during the first two months after spring spawning in the Northeast Atlantic. Horizontal behavior is modelled as passive advection driven by daily GLORYS velocity fields (current speed and direction). We do not include directional horizontal swimming, which can affect larval dispersal (Cresci et al., 2025), because species-specific information on the ontogeny of active horizontal swimming in blue whiting larvae is lacking, and has not previously been included in larval blue whiting drift studies (Bartsch and Coombs, 1997; Laiz et al., 2025). Vertical behavior is parameterized from observations. Agents are released randomly between 300–400m, consistent with spawning over deep water west of the British Isles and with the reported depth range of eggs and yolk-sac larvae (Bartsch and Coombs, 1997; Ådlandsvik et al., 2001; Miesner and Payne, 2018; Miesner et al.,

2022). Eggs are neutrally buoyant at spawning depths, and most hatch after about five days of incubation (Coombs and Hiby, 1979). After hatching, larvae begin a gradual ascent, reaching the upper ~0–60 m of the water column by roughly two weeks post-spawning (Ådlandsvik et al., 2001). The velocity fields in GLORYS do not include a vertical velocity component. However, we add a weak stochastic vertical dispersion (random-walk) with a standard deviation of vertical speed on the order of  $10^{-5} \text{ ms}^{-1}$  to represent small-scale processes such as microturbulence and individual variability not explicitly resolved by the hydrodynamic fields (Visser, 1997). This provides minimal vertical dispersion without imposing diel migration. Simulated vertical behavior of agents during the first month since release is shown in [Supplementary Figure 18](#).

Agent dispersal is simulated for two months post-spawning. Beyond 60 days, larvae might develop swimming ability and initiate diel vertical migration, reducing the realism of a purely passive formulation. The pelagic larval phase is estimated to last up to about two months, encompassing the critical early life period when environmental variability strongly influences survival and subsequent recruitment dynamics (Bailey and Heath, 2001). This two-month window is consistent with the simulated drift period used in a recent Lagrangian modelling study of blue whiting larvae (Laiz et al., 2025).

Spawning release locations ([Figure 1](#)) are selected to cover the principal blue whiting spawning grounds west of the British Isles (Trenkel et al., 2014; Miesner et al., 2022; ICES, 2022, 2024). We divide the spawning grounds into four areas - Porcupine Bank, Rockall Trough, Rockall Plateau, and the Hebrides - to quantify how initial position influences subsequent transport and retention of blue whiting larvae. The reported depth of egg release and vertical distribution in literature (see references above) and its representation in our model setup (i.e., 300–400 m) implies that regions shallower than 300 m within these areas (e.g., on top of Rockall Plateau and Porcupine Bank) are effectively excluded as potential spawning grounds.

Mortality processes are not included in the model. Predation and starvation are potentially important but would require spatio-temporal fields of prey and predator distributions, which are beyond the scope of this study. We therefore interpret outcomes strictly in terms of passive drift and analyze how transport affects the dispersal of blue whiting larvae. Details of the ABM equations, parameter values, and numerical settings are provided in the Supplementary Material.

### 2.2.3 Simulations: selection of years and spawning periods

We select simulation years based on extremes of blue whiting  $\ln R/SSB$  during 1993–2021. Six high years (1995, 1996, 2000, 2014, 2020, 2021) and six low years (2005, 2006, 2007, 2008, 2017, 2018) are identified ([Figure 3](#)). Years close to the long-term mean  $\ln R/SSB$  are not included, as our aim is to compare transport conditions during extreme  $\ln R/SSB$  years.

Two-month simulations are run for each of the 12 years, starting on 1 March and ending on 1 July, with a model time step

of 30 min. Blue whiting spawn most intensively during March-May (Hátún et al., 2009b; Pointin and Payne, 2014; Miesner and Payne, 2018; Miesner et al., 2022; ICES, 2022, 2024). Accordingly, agents are released on three dates per year (1 March, 1 April, 1 May). Agents are released on the MIKE 3 FM unstructured mesh by seeding one agent per grid cell inside the four spawning polygons at locations where water depth exceeded 300 m. This results in 7946 particles per release date (i.e., the number of grid cells within the spawning areas), and 23838 particles per year (three release dates), similar to the per-year particle numbers used by Jansen et al. (2021).

## 2.2.4 ABM outputs, analyses, sensitivity tests

From the ABM particle-tracking outputs, we extract five metrics that describe the magnitude and direction of the transport experienced by the agents; we quantify dispersal and retention indices, as described below.

We calculate net displacement (km) of a particle as the great-circle (haversine) horizontal distance between release position and final position.

The dispersal index (%) is computed as (net displacement/accumulated distance)  $\times$  100, where accumulated distance is the cumulative path length obtained by summing stepwise great-circle distances between successive 30-min positions along the trajectory. Higher dispersal index values ( $\sim$ 100%) indicate straighter trajectories; lower values ( $\sim$ 0%) indicate more meandering and higher retention.

We compute the directional components of net displacement using haversine distances (km) projected along longitude ( $\Delta x$ , east-west) and latitude ( $\Delta y$ , north-south). We adopt the sign convention  $\Delta x > 0$  eastward,  $\Delta x < 0$  westward;  $\Delta y > 0$  northward,  $\Delta y < 0$  southward.

We define the retention index (%) as the percentage of agents whose final positions lie within their own spawning area, relative to the number of agents released from that area.

We compute the ABM transport metrics one and two months after release and average them across spawning days for each release area. We summarize these metrics as mean  $\pm$  2  $\times$  standard error (SE) averaged across all 12 simulation years and, separately, for the six high and six low extremes in R/SSB years. We test whether the high-low contrasts in the five ABM transport metrics for each spawning area and time since release differ significantly after Bonferroni correction ( $p_{adj} < 0.05$ ; 40 tests = 5 metrics  $\times$  4 areas  $\times$  2 intervals).

For each spawning area, we then build time series of each ABM transport metric for the 12 simulation years and use these to fit linear regression models testing whether variation in blue whiting ln R/SSB can be explained by the transport conditions experienced by eggs and larvae. We also correlate ln R/SSB with the SPG, WSC and Q indices for the same 12 years considered for the ABM simulations.

We conduct sensitivity tests to evaluate the robustness of the results to key parameters and assumptions for a high-recruit-per-spawner year (2021) and a low-recruit-per-spawner year (2006). First, we test the sensitivity of drift patterns to the vertical

distribution and behavior of the modelled eggs and larvae by running two additional scenarios in which agents are constrained either to the surface layer (upper 10 m) or to deeper waters ( $\sim$ 350 m) during the entire simulation period (i.e., 2 months), and we compare these results with the simulated vertical-behavior configuration. Second, we vary the day of release by comparing simulations with agents released on the 1<sup>st</sup>, 5<sup>th</sup>, 10<sup>th</sup>, 15<sup>th</sup>, 20<sup>th</sup>, and 25<sup>th</sup> day of each month during March-May; these simulations evaluate the possible temporal variation during the main spawning season of flows and transports. Finally, we examine the influence of the drift duration by extracting transport metrics after one, two, three, and four months since release (for agents released on 1 March only). Results of the sensitivity analyses are described in the [Supplementary Material](#).

## 3 Results

### 3.1 Transport analyses

#### 3.1.1 Ellett Line transport: climatology and interannual variability (1993–2020)

Annual volume transport estimates (Q) across the EL are predominantly positive for all four indices (ELA100, ELA400, ELBC100, ELBC400), indicating net northward flow across both transects A and BC (Figures 2A, B). Mean transport is substantially (ca. 3-10-fold) larger across transect A than BC at both depth ranges (means  $\pm$  standard deviation, 1993-2020): ELA100 =  $1.1 \pm 0.3$  Sv and ELA400 =  $4.5 \pm 1.0$  Sv; ELBC100 =  $0.1 \pm 0.4$  Sv and ELBC400 =  $1.6 \pm 1.3$  Sv (Figure 2B). As expected, depth-integrated transports to 400 m are larger than those to 100 m on each transect, reflecting the additional contribution from deep-layer flows. Interannual variability is pronounced but no temporal trend is evident in any time series over 1993-2020 (Figure 2A). Two years stand out on the BC section (1997 and 2015), when transport weakens sharply and turns southward (negative), in contrast to the consistently northward flow across transect A.

Seasonal (March-May) transport estimates show the same overall pattern as the annual means -predominantly northward flow with substantially stronger transport across transect A than BC -although the strong southward anomaly on BC evident in the annual series in 1997 and 2015 is only present in 1997 in the spawning-season series (Supplementary Figure 3, S4).

A visual inspection of the time series of annual transport across EL transect A from 0–100 m (Q ELA100) and ln R/SSB shows that the two indices share some multi-annual variability during 1993-2020 (Figure 2C). The regression of ln R/SSB on Q ELA100 over the 28-year period is positive ( $R^{2adj} = 0.22$ ,  $p = 0.006$ ; Figure 2D), indicating higher recruit per spawner in years with stronger northward flow across the Hebrides-Rockall Trough. This co-variation is supported by quantitative statistical analyses as described below.

TABLE 1 Model performance metrics for all fitted recruit per spawner (ln R/SSB) – annual transport (Q) models. .

Model	EL Transect	Covariate (s)	Residual structure	<i>k</i>	<i>df</i>	AICc	logLik	$\Delta_i$	ER
GM	–	Intercept	Independent	1	2	74.57	-35.05	0	1
A1	–	Intercept	AR(1)	2	3	59.70	-26.35	14.87	1693
Q ELA100	A	Intercept + Q EL A 100	Independent	2	3	68.97	-30.98	5.61	17
<b>Q ELA100 A1</b>	<b>A</b>	<b>Intercept + Q ELA100</b>	<b>AR(1)</b>	<b>3</b>	<b>4</b>	<b>58.40</b>	<b>-24.33</b>	<b>16.17</b>	<b>3244</b>
Q ELA400	A	Intercept + Q ELA400	Independent	2	3	74.60	-33.80	<0	<1
Q ELA400 A1	A	Intercept + Q ELA400	AR(1)	3	4	59.92	-25.09	14.65	1517
Q ELBC100	BC	Intercept + Q ELBC100	Independent	2	3	76.56	-34.78	<0	<1
Q ELBC100 A1	BC	Intercept + Q ELBC100	AR(1)	3	4	62.44	-26.35	12.13	431
Q ELBC400	BC	Intercept + Q ELBC400	Independent	2	3	76.79	-34.90	<0	<1
Q ELBC400 A1	BC	Intercept + Q ELBC400	AR(1)	3	4	62.43	-26.34	12.14	433

Elett Line (EL) transect indicates section A or BC. Covariate(s) list the fixed effects: Intercept and the annual transport indices Q (ELA100, ELA400, ELBC100, ELBC400). Residual structure: Independent = residuals assumed independent (no temporal autocorrelation); AR(1) = first-order autoregressive residual correlation. *k* is the number of estimated parameters (including fixed and random effects). *df* is the degrees of freedom. AICc is the small-sample-corrected Akaike Information Criterion. logLik is the maximized log-likelihood.  $\Delta_i$  is the difference in AICc from the GM model. Evidence ratio ER =  $\exp(\Delta_i/2)$  gives each model's support relative to GM.  $\Delta_i > 0$  and ER > 1 indicate model is better than GM. The model with the best overall goodness of fit (i.e., lowest AICc) is shown in bold.

### 3.1.2 Recruit per spawner and transport relationships (1993–2020)

Model performance metrics for all fitted recruit per spawner (ln R/SSB) and Q annual models are shown in Table 1. Comparing AICc to the GM baseline shows that models using EL A transport outperform those using EL BC transport at both 0–100 m and 0–400 m. The best overall fit is the model that uses Q across EL A at 0–100m as covariate and includes a first-order autoregressive (AR(1)) residual correlation (Q ELA100 A1; AICc = 58.40;  $\Delta_i$  = 16.17; ER = 3244). The next best is the AR(1)-only model (A1; AICc = 59.70;  $\Delta_i$  = 14.87; ER = 1693), followed closely by the AR(1) model with EL A 400 transport (Q ELA400 A1; AICc = 59.92;  $\Delta_i$  = 14.65; ER = 1517). AR(1) models with EL BC transports also improve over GM but with smaller gains ( $\Delta_i$  ~ 12; ER ~ 431–434). Among models with independent residuals (no temporal autocorrelation), Q ELA100 shows a modest improvement over GM ( $\Delta_i$  = 5.61; ER = 16.5), whereas Q ELA400, Q ELBC100, and Q ELBC400 do not ( $\Delta_i$  < 0; ER < 1). Time series and scatter plots for 1993–2020 of ln R/SSB and each Q annual index are shown in Supplementary Figure 2.

Consistent with the annual-flow results, models using spawning-season transport across transect A (especially ELA100 with AR(1) residuals) provide the best fit to ln R/SSB, whereas seasonal transport across transect BC shows weaker and less consistent associations (Supplementary Table 1).

## 3.2 ABM analyses

To illustrate spatial patterns of larval drift, we first map the positions of all agents after two months since release, colored by

their accumulated distance travelled (cumulative path length along each trajectory). Figure 4 highlights these patterns for Porcupine Bank and the Hebrides in contrasting high- and low-recruit-per-spawner (ln R/SSB) years, where differences are most pronounced, whereas supplementary figures (Supplementary Figures S19–S21) show the corresponding maps for all spawning areas and all 12 simulation years. To further support visualization of the drift pathways, we extract videos of ABM particle trajectories showing 50 agents from all spawning areas for the 2014 simulation, as well as all agents released on 1 March from Porcupine Bank and the Hebrides during a high- (2020) and a low- (2006) recruit-per-spawner year. These videos are available in the following GitHub repository: [https://github.com/costanzacappelli/BlueWhiting\\_Transport](https://github.com/costanzacappelli/BlueWhiting_Transport).

Below, we summarize the dispersal and retention patterns derived from these simulations.

### 3.2.1 ABM particle-tracking outputs: dispersal and retention during 12 extreme recruit-per-spawner years

Across high and low ln R/SSB years, mean displacement (km) of particles ranges from ~101–164 km one month and ~151–228 km two months after agent release date (Figure 5). Mean values  $\pm$  2SE over 12 years show that at two months, displacement is largest from Rockall Trough ( $226 \pm 8$  km), followed by the Hebrides ( $196 \pm 9$  km), and Rockall Plateau ( $172 \pm 7$  km), while agents from Porcupine Bank travel shorter distances ( $157 \pm 6$  km) (Supplementary Figure 22). Contrasts of transport distance in high-low ln R/SSB years are most evident at the Hebrides:

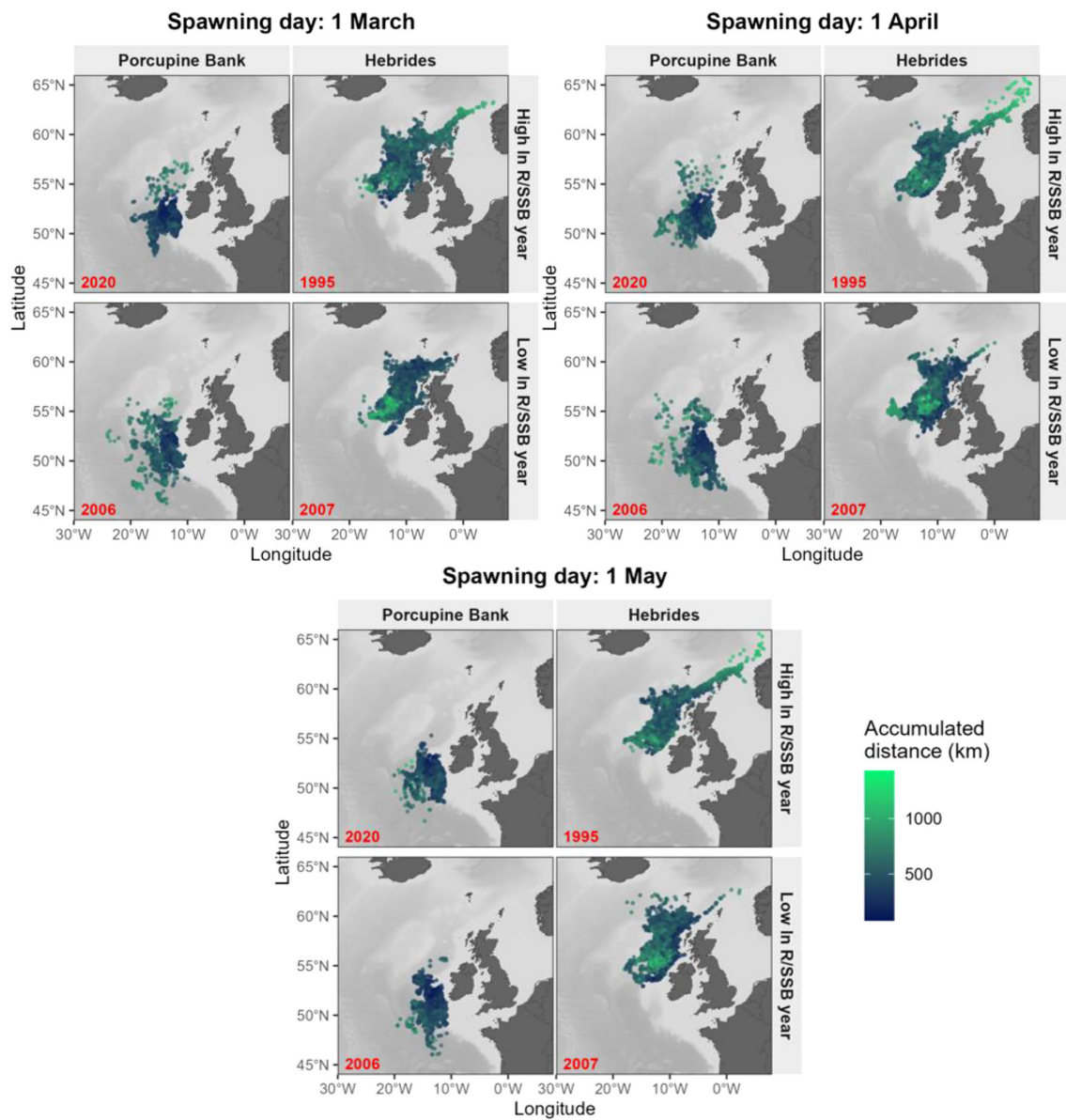


FIGURE 4

ABM particle-tracking outputs showing the positions of simulated blue whiting eggs and larvae two months after release from Porcupine Bank and the Hebrides during years of high- (2020, 1995) and low- (2006, 2007) recruit per spawner ( $\ln R/SSB$ ). Larval drift maps are shown separately for each spawning day (1 March, 1 April, 1 May). Agents are colored by the accumulated distance travelled (km) during the two-month drift (i.e., the cumulative path length obtained by summing stepwise distances between successive 30-min locations along each trajectory). Porcupine Bank: particles are highly retained over the bank in 2020, whereas in 2006 particles show a modest southward drift. Hebrides: in 1995, particles experience intense northward transport toward the Faroese and Norwegian Seas along relatively straight pathways, while in 2007 drift is more meandering and dominated by mesoscale eddy-driven recirculation, as indicated by high accumulated distances for particles that remain relatively close to their release area.

displacement is higher in the high  $\ln R/SSB$  years at one month ( $128 \pm 3$  km) and two months ( $206 \pm 10$  km) than in low  $\ln R/SSB$  years ( $119 \pm 4$  km and  $187 \pm 11$  km at one and two months, respectively). Porcupine Bank shows the opposite pattern at two months, with greater displacement in low  $\ln R/SSB$  years ( $163 \pm 8$  km) than in high  $\ln R/SSB$  years ( $151 \pm 6$  km; Figure 5).

The dispersal index (%), expressed as (net displacement/accumulated distance)  $\times 100$ , decreases from one to two months post-release in all areas, indicating increasingly meandering trajectories with time (Figure 5). Across areas and in both high

and low  $\ln R/SSB$  years, one-month means span  $\sim 45$ – $54\%$ , and two-month means  $\sim 33$ – $42\%$ . Considering means  $\pm 2$ SE across all 12 years (Supplementary Figure 22), Rockall Plateau shows the highest dispersal index at both one month ( $54 \pm 2\%$ ) and two months ( $42 \pm 2\%$ ), while Rockall Trough is lowest ( $46 \pm 2\%$  at one month;  $34 \pm 2\%$  at two months). Porcupine Bank (PB) and the Hebrides (H) are intermediate: one month (PB:  $49 \pm 2\%$ , H:  $47 \pm 2\%$ ); two months (PB:  $36 \pm 1\%$ , H:  $37 \pm 2\%$ ). High-low contrasts are most pronounced at the Hebrides: the dispersal index is higher in high  $\ln R/SSB$  years at both one month ( $49 \pm 3\%$  vs  $45 \pm 1\%$ ) and two

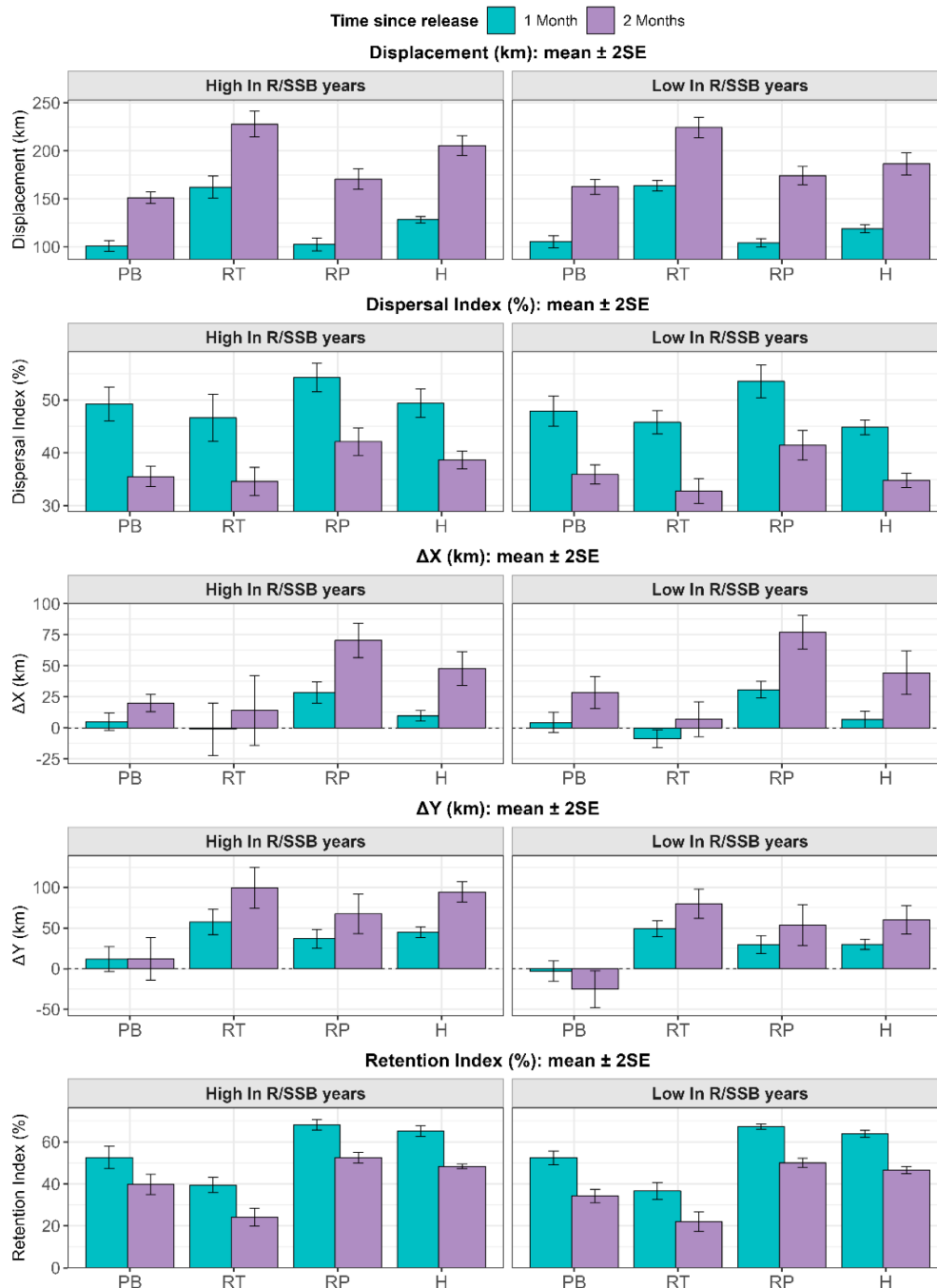


FIGURE 5

Mean  $\pm$  2 x standard error (SE) of ABM-derived transport metrics for the 12 simulation years, shown separately for high and low ln R/SSB years. Metrics include displacement (km), dispersal index (%), east-west transport ( $\Delta x$ , km), north-south transport ( $\Delta y$ , km), and retention index (%), calculated after one month (blue) and two months (purple) since release for each spawning area (PB = Porcupine Bank, RT = Rockall Trough, RP = Rockall Plateau, H = Hebrides). Of the 40 high-low contrasts tested, only 6 are significant after Bonferroni correction ( $p_{adj} < 0.05$ ). See Methods for definitions of metrics.

months ( $39 \pm 2\%$  vs  $35 \pm 1\%$ ). In the other three spawning areas, differences between high and low years are small, and the  $\pm$  2SE intervals overlap at both one and two months (Figure 5).

Mean  $\pm$  2SE north-south transport ( $\Delta y$ , km) across the 12 years is highest from Rockall Trough ( $53 \pm 9$  km at one month,  $90 \pm 16$  km at two months) and the Hebrides ( $38 \pm 6$  km at one month,  $77 \pm 15$  km at two months), indicating persistent northward drift from these areas (Figure S22). Rockall Plateau shows intermediate

northward transport ( $33 \pm 8$  km at one month,  $61 \pm 17$  km at two months), Porcupine Bank displays near-zero or slightly southward movement ( $4 \pm 10$  km at one month,  $-6 \pm 20$  km at two months). High-low ln R/SSB contrasts in  $\Delta y$  are most evident at the Hebrides and Porcupine Bank. At the Hebrides,  $\Delta y$  is greater in high ln R/SSB years at both one month ( $45 \pm 7$  km vs  $30 \pm 6$  km) and two months ( $94 \pm 13$  km vs  $60 \pm 18$  km) relative to low R/SSB years. At Porcupine Bank,  $\Delta y$  is weakly northward in high ln R/SSB

years ( $12 \pm 15$  km at one month;  $12 \pm 26$  km at two months) but is southward in low R/SSB years ( $-3 \pm 13$  km at one month;  $-25 \pm 23$  km at two months; Figure 5).

East-west transport ( $\Delta x$ , km) across all 12 simulations is generally weak to moderate after one month and strengthens by two months, particularly eastward from Rockall Plateau ( $74 \pm 10$  km) and the Hebrides ( $46 \pm 11$  km; mean  $\pm$  2SE; Supplementary Figure 22).  $\Delta x$  from Porcupine Bank and Rockall Trough is comparatively weaker ( $24 \pm 7$  km and  $11 \pm 15$  km, respectively, at two months). Differences between high and low ln R/SSB years are small across all spawning areas, and no consistent contrast is evident in  $\Delta x$  (Figure 5).

Retention index (%) varies strongly among spawning areas and decreases with time since release. Across all 12 years, one-month means range from 38% to 68%, while two-month means drop to 23–51% (Supplementary Figure 22). Rockall Plateau shows the highest retention (one month:  $68 \pm 1\%$ ; two months:  $51 \pm 2\%$ ), followed by the Hebrides (one month:  $64 \pm 2\%$ ; two months:  $47 \pm 1\%$ ), while Rockall Trough has the lowest (one month:  $38 \pm 3\%$ ; two months:  $23 \pm 3\%$ ). Porcupine Bank shows intermediate values (one month:  $53 \pm 3\%$ ; two months:  $37 \pm 3\%$ ). High-low ln R/SSB contrasts are

evident at Porcupine Bank, where retention after two months is  $40 \pm 5\%$  in high years and  $34 \pm 3\%$  in low years. Differences at other locations and time intervals are smaller and generally fall within the 2SE confidence bounds (Figure 5).

Significance tests of the high-low ln R/SSB contrasts for all five ABM transport metrics show that only 6 of 40 tests are significant after Bonferroni correction ( $p_{adj} < 0.05$ ), and these occur only at two spawning areas. At the Hebrides, high ln R/SSB years have a significantly higher dispersal index at one and two months, and greater displacement and stronger northward transport ( $\Delta y$ ) at two months, compared to low ln R/SSB years. At Porcupine Bank, northward transport ( $\Delta y$ ) and retention index after two months since release are both significantly higher in high than in low ln R/SSB years. All remaining high-low contrasts are not significant ( $p_{adj} > 0.05$ ).

### 3.2.2 Recruitment and ABM outputs covariations for 12 extreme recruit-per-spawner years

To assess whether interannual variability in blue whiting recruitment is associated with differences in dispersal and

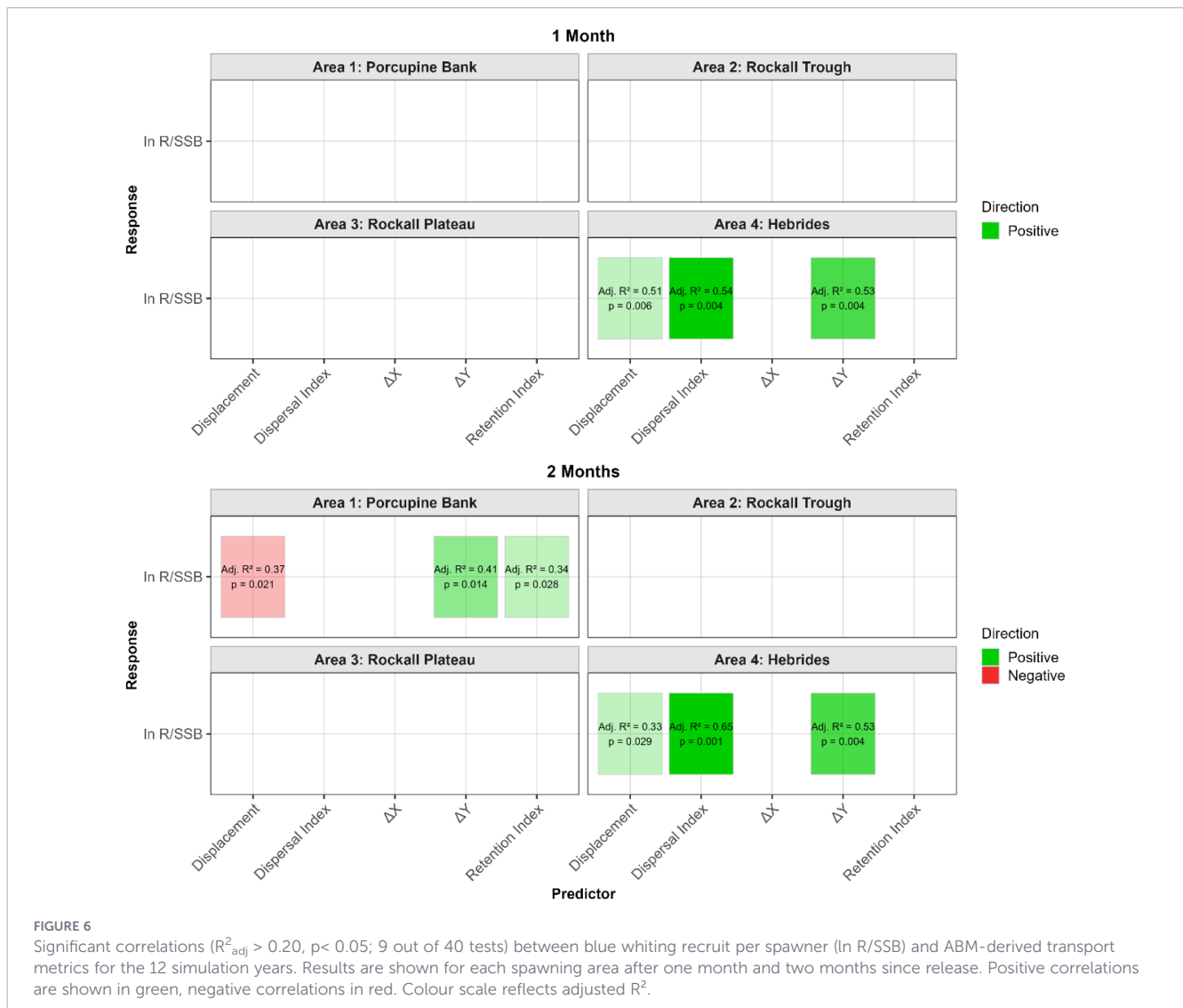


**FIGURE 6** Significant correlations ( $R^2_{adj} > 0.20$ ,  $p < 0.05$ ; 9 out of 40 tests) between blue whiting recruit per spawner (ln R/SSB) and ABM-derived transport metrics for the 12 simulation years. Results are shown for each spawning area after one month and two months since release. Positive correlations are shown in green, negative correlations in red. Colour scale reflects adjusted  $R^2$ .

retention patterns experienced by early life stages, we regress  $\ln R/SSB$  against the five ABM-derived transport metrics for each spawning area for the 12 simulation years (Figure 6). We find 9 significant correlations ( $R^{2adj.} > 0.20$ ,  $p < 0.05$ ) out of 40 tested (5 metrics  $\times$  4 areas  $\times$  2 intervals), all for agents released from the Hebrides or Porcupine Bank. At the Hebrides,  $\ln R/SSB$  covaries positively with displacement, dispersal index, and  $\Delta y$  at one month ( $R^{2adj.} = 0.51$ – $0.54$ ), and with displacement ( $R^{2adj.} = 0.33$ ), dispersal index ( $R^{2adj.} = 0.65$ ), and  $\Delta y$  ( $R^{2adj.} = 0.53$ ) at two months since release. At Porcupine Bank,  $\ln R/SSB$  is negatively related to displacement ( $R^{2adj.} = 0.37$ ) but positively related to northward transport and retention after two months ( $R^{2adj.} = 0.34$ , and  $R^{2adj.} = 0.41$  respectively). No significant relationships are detected for Rockall Trough or Rockall Plateau.

Supplementary figures show time series and scatter plots of the significant correlations between  $\ln R/SSB$  and ABM transport metrics shown in Figure 6, only for 2 months since agents release (Hebrides: Supplementary Figure 23; Porcupine Bank: Supplementary Figure 24). Supplementary Figure 25 shows the correlations between  $\ln R/SSB$  and the ocean-climate indices (SPG, WSC, Q) for the 12 years selected for the ABM simulations. Sensitivity tests on ABM parameters and assumptions are illustrated and discussed in the Supplementary Material (vertical behavior: Supplementary Figure 26, S27; spawning day: Supplementary Figure 28, S29; drift duration: Supplementary Figure 30, S31). Notably, spawning-day sensitivity tests indicate that ABM transport metrics are generally stable across March–May, apart from a few late-season outliers (late April–May; most evident in 2021) showing episodic spikes in dispersal and sharp drops in retention (Supplementary Figure 29).

## 4 Discussion

Our study combines multidecadal transport analyses and agent-based simulations to investigate how ocean circulation affects the survival of the early life stages of blue whiting in the Northeast Atlantic Ocean. Northward flow across the Ellett Line transect A, spanning the Hebrides and Rockall Trough, is the most informative oceanographic predictor of recruitment over the 28 years (1993–2020) investigated here. After accounting for significant temporal autocorrelation in the  $R/SSB$  data, stronger poleward flow across this transect, especially in the upper 0–100 m, corresponds to higher recruit per spawner, whereas transport across the western BC transect over Rockall Plateau shows no consistent relationship. Complementing these findings, the ABM simulations for the 12 extreme recruit-per-spawner years indicate that high-recruit-per-spawner years coincide with stronger northward export and straighter trajectories of eggs and larvae along the slope current from the Hebrides, as well as with strong local retention over Porcupine Bank. Together, these results suggest that both directional advection and local retention act as key modulators of blue whiting early life survival, influencing the spawning-nursery area connectivity with potential consequences on yearclass strength; however, the importance of retention or dispersal differs among

these two spawning areas. By highlighting the specific flow regimes that favor recruitment in specific spawning areas, our study provides a mechanistic interpretation of the link between ocean-climate variability in the Northeast Atlantic Ocean and blue whiting recruitment success.

### 4.1 Magnitude and pattern of Ellett Line transport 1993–2020

The transport indices derived here highlight a pronounced east-west contrast of flow across the Rockall Trough – Rockall Plateau region. Mean transport between 1993 and 2020 is substantially larger and northward along the Hebrides-Rockall Trough (transect A) than across the Rockall Plateau (transect BC). This east-west contrast agrees with previously published hydrographic and mooring transport estimates across the Ellett Line. Repeated sections through Rockall Trough for 1975–1998 show a mean poleward transport of Eastern North Atlantic Water of  $3.7 \pm 2.4$  Sv above 1200 m of which 3 Sv is carried by the shelf edge current (Holliday et al., 2000). More recently, as part of the Overturning in the Subpolar North Atlantic Programme (OSNAP), continuous moorings report a four-year (2014–2018) mean northward transport of 6.6 Sv by the NAC in the east and interior of the Rockall Trough, while a mean southward transport of  $-2.0$  Sv is observed in the west of the basin (Houpert et al., 2020).

Our indices reveal a pronounced drop along the A transect in 2017, when the annual mean transport in the 0–400 m layer declines sharply by roughly 2 Sv. A comparable reduction ( $\sim 3$  Sv) is seen in the Rockall Trough transport derived from the OSNAP mooring array for the same year (Houpert et al., 2020). The OSNAP array spans 21 stations of the Extended Ellett Line (stations S-IB1), all of which are included in our A transect that extends further east and covers 36 stations (1G-A). Although these literature values involve different depth integrations and sampling periods, they show that the slope current is the dominant northward pathway, whereas the NAC branch over Rockall plateau is weaker or even southward. Our higher transport on transect A relative to transect BC reflects the same dynamical pattern as seen in the OSNAP array.

Building on this east-west contrast, further statistical analyses show that the recruit per spawner relationship including transport across transect A in the upper 0–100 m provides the lowest  $AIC_c$  and therefore the best fit to the recruit per spawner data, in comparison with models using transport across transect BC; those models only explain similar levels of variability as the long-term geometric mean (Table 1). The same pattern is observed using the spawning season transport indices, although the associated improvements in model fit are smaller than for the corresponding annual averages (Supplementary Table 1). This stronger linkage between annual flows and recruit per spawner may reflect uncertainty in the exact timing of peak spawning in each year and spawning area, or it may indicate that transport conditions outside the core spawning season precondition the system by influencing vertical mixing, Taylor-column stability, and trophic productivity that subsequently affect larval survival. New observational and modelling studies will be needed to investigate these possibilities in more detail.

Current velocity through the Trough further support the east-west contrast: significant positive correlations between flow velocity and recruit per spawner are confined to the eastern longitudes ( $\sim 6\text{--}9^\circ$  W) of transect A near the continental slope at depths  $\sim 0\text{--}150$  m. These relationships are more pronounced for the annual velocity means than for the seasonal averages, suggesting that the longer-term mean flow along the Hebrides slope is the component most strongly linked to blue whiting productivity (Supplementary Figure 16). These patterns suggest that advection along the slope current is critical for survival of blue whiting early life stages. We envisage that if our transect A was restricted to the slope region, the flow-recruitment correlations would likely be even stronger.

## 4.2 Dispersal and retention patterns from the ABM simulations

Our agent-based simulations reveal distinct spatial patterns in drift and retention of blue whiting eggs and larvae among spawning areas during the first two months post-spawning. At the Hebrides, high-recruit-per-spawner years are characterized by larger net displacement, higher dispersal index (straighter trajectory) and stronger northward transport relative to low-recruit-per-spawner years (Figure 5). This pattern indicates that eggs and larvae released at the Hebrides benefit from rapid advection along the slope current and are efficiently transported to nursery grounds in the Norwegian Sea, Northern North Sea, and toward the Faroe waters. Porcupine Bank exhibits the opposite pattern and is characterized by weak northward drift, with particles experiencing near-zero or even slightly southward transport. This region lies close to the long-term mean WSC zero-line (Cappelli et al., 2025). During high-recruit-per-spawner years, agents released from Porcupine Bank area display lower net displacement and significantly higher retention than in low-recruit-per-spawner years, when agents are transported further south (Figure 5). This pattern suggests that larvae spawned at Porcupine Bank survive better when retained near their spawning grounds, at least during the first two months of life.

These relationships are statistically supported in both areas, with recruit per spawner significantly increasing with strong northward transport from the Hebrides and with higher retention at Porcupine Bank (Figure 6).

The spatial pattern of larval drift revealed by our ABM simulations is consistent with earlier particle-tracking studies. The numerical circulation and transport model of Bartsch and Coombs (1997), which used a coarser horizontal resolution ( $\sim 20$  km) than ours ( $\sim 9 \times 7$  km), similarly showed that blue whiting larvae during 1994 and 1995 are either transported northward along the shelf edge into the northern North Sea and Norwegian Sea or retained in the Rockall Gyre and over Porcupine Bank. Our findings also align with recent Lagrangian simulations by Laiz et al. (2025). They linked the extraordinary numbers of blue whiting recruits observed in survey data from Porcupine Bank in 2020 to a persistent Taylor column circulation over the Bank, driven by unusually weak wind mixing. This anticyclonic circulation enhanced phytoplankton accumulation, likely increasing food availability for larvae, and acted as a retention mechanism for both larvae and prey. Field

observations support this interpretation: during a 1994 survey, blue whiting larvae retained above Porcupine Bank within cooler, less saline waters associated with an anticyclonic circulation fed predominantly on larger calanoid nauplii, whereas larvae in the adjacent warm, saline shelf-edge current relied mainly on smaller cyclopoid nauplii, indicating a more favorable feeding environment over the bank (Hillgruber and Kloppmann, 1999). While our model does not explicitly include chlorophyll or prey fields, it indicates that similar retention-productivity coupling may occur in other years: high recruit per spawner coincides with periods of high retention at Porcupine Bank, suggesting that larvae benefit from prolonged residence in nutrient-rich waters. It is also likely that retention in the coastal areas (Porcupine Bank area and further north) might enhance survival of blue whiting larvae, possibly due to lower predation pressure by mackerel that spawn in the surface layers in offshore waters west of Ireland and Scotland, as suggested by Payne et al. (2012).

Overall, our simulations generally reveal high retention across the entire spawning domain, but with some transport from and dispersal among different individual spawning areas. Dispersal indices generally decrease from one to two months in all areas, indicating that larvae experience increasingly meandering trajectories over time. This pattern reflects the strong mesoscale activity characteristics of the Northeast Atlantic, a region dominated by eddies and recirculation features (Ullgren and White, 2012; Verezemskaya et al., 2021). Our two-month retention index values are higher at the Rockall Plateau ( $51 \pm 2\%$ ) than at Porcupine Bank ( $37 \pm 3\%$ ), consistent with earlier Lagrangian modelling studies that also found greater retention over the Rockall Plateau (78–86%) than over Porcupine Bank (45–69%) (Bartsch and Coombs, 1997; Skogen et al., 1999).

## 4.3 Role of basin-scale circulation: SPG-NAC influence on transport and larval drift

Considering our results in the context of large-scale ocean circulation, they align closely with the known influence of the SPG and the NAC on regional transport pathways. Supplementary analyses indicate that only the flow (Q) along transect A is tightly coupled to basin-scale circulation as represented by the SPG index, whereas transport across transect BC appears to be driven primarily by local recirculation. Among all transport indices considered in our In R/SSB-Q models, only the flows across transect A show a significant relationship with SPG (Supplementary Figure 5; Supplementary Table 2). Current velocity through the Ellett Line reinforce this pattern: significant velocity-SPG correlations are confined to the eastern part of the section ( $\sim 6\text{--}9^\circ$  W) near the Hebrides slope, with no comparable signal over Rockall Plateau (Figure S16). This suggests that transport along transect A captures variability in the main NAC branch flowing across Rockall Trough and along the European shelf break, which represents the southern and eastern edge of the SPG circulation, whereas flow across BC largely reflects anticyclonic recirculation and mesoscale eddy activity over Rockall Plateau (Gary et al., 2018; Houpert et al., 2020).

Variations in the strength and position of the SPG lead to corresponding shifts in the NAC's transport pathway and properties, especially in the region west of the British Isles (Holliday, 2003; Häkkinen and Rhines, 2004; Hátún et al., 2005; Holliday et al., 2020; Houpert et al., 2020). A strong and expanded SPG steers the NAC eastward into the Rockall Trough and intensifies poleward inflow of cold and relatively fresh subarctic waters along the Hebrides slope. Conversely, as the SPG weakens and shifts westward, the subpolar front retreats westward and warmer, saltier subtropical waters can spread northward and westward in the Rockall Plateau, resulting in a reduced NAC transport towards Rockall Trough and along the continental shelf. This pattern is reflected in both our Q-SPG models and velocity-SPG correlation transects (Supplementary Figure 5 and S16; Supplementary Table 2).

The absence of a SPG signal in BC transport, which is characterized by a weaker flow and occasionally sharp negative anomalies (1997 and 2015), indicates that flow over Rockall Plateau is decoupled from gyre dynamics and instead dominated by eddy-driven recirculation (Houpert et al., 2020). Eddy-resolving analyses and satellite altimetry show that the western Rockall Plateau (~20° W) is a hotspot of mesoscale eddy generation, where cyclones and anticyclones recirculate NAC waters around Hatton-Rockall Plateau and can even reverse the mean flow (Ullgren and White, 2012; Verezemskaya et al., 2021). The large drops in Q across the BC section during certain years likely reflect such temporary retroflexion of the NAC's western branch around the Rockall Plateau region (Gary et al., 2018; Houpert et al., 2020), suggesting that larval transport from offshore spawning grounds is more susceptible to local circulation features than to basin-scale forcing.

These basin-scale circulation patterns align with our ABM findings. Particle tracking simulations show that high-recruit-per-spawner years are characterized by stronger and more directed northward transport of larvae from the Hebrides region (Figures 4, 5). For example, in the 12 extreme recruit-per-spawner years we simulated, blue whiting recruit per spawner is positively correlated with the SPG index (Supplementary Figure 25). We suggest that a strong SPG, and the associated NAC strengthening along the slope, enhances early survival via favorable transport pathways.

This mechanism suggests that observed shifts in the distribution of blue whiting spawners and early stage larvae (i.e., < 6 mm) under different gyre states (Hátún et al., 2009b; Miesner and Payne, 2018) could have consequences for the trajectories of eggs and larvae produced in different areas in different years. These previous studies have shown that when the SPG is strong and spreads cold and fresh subpolar waters eastward, spawning remains constrained to the European continental slope (as well as to the southern Porcupine Bank), where eggs and larvae enter the NAC (Hátún et al., 2009b; Miesner and Payne, 2018). In contrast, a weak and contracted SPG allows warm, saline subtropical waters to penetrate farther north along the European shelf and westward over Rockall Plateau, and the spawning grounds expand to these areas (Hátún et al., 2009b; Payne et al., 2012; Miesner and Payne, 2018).

Our results suggest that such offshore spawning during weak-gyre periods may be suboptimal for recruitment. Larvae released over the Rockall Plateau tend to experience more meandering,

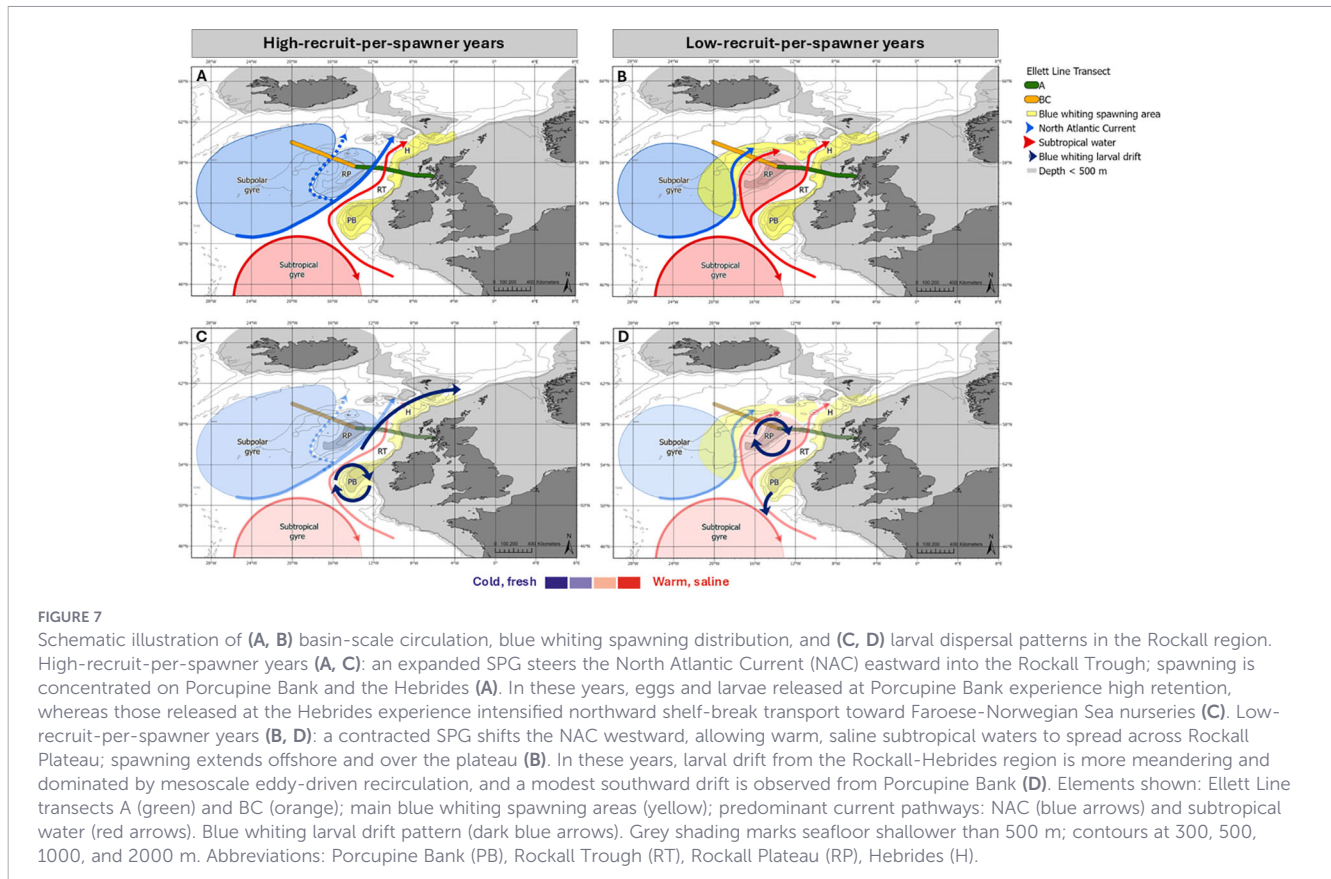
recirculating trajectories with limited connectivity to known nursery areas, as reflected by the lack of recruitment link with transport across the plateau. A weakened SPG has been associated with reduced nutrient concentrations, diminished productivity and reduced zooplankton energy content in the Northeast Atlantic (Johnson et al., 2013; Tyldesley et al., 2024), implying that even if the spawning habitat expands westward, larval survival may be limited by unfavorable transport conditions and retention in a nutrient-poor environment.

Conversely, when spawning is restricted to the European continental slope under a strong SPG regime, larvae benefit from rapid poleward advection along the NAC, and increased mixing of nutrients to the surface layer due to interaction of flows with bathymetry (e.g., shelf edge, seamounts, banks, channels (Holliday et al., 2008, 2020; Hátún et al., 2021)). These conditions likely enhance effective transport to nursery grounds and improve the trophic environment experienced by early life stages during this drift, as reflected by higher recruit per spawner observed under strong gyre regimes and intensified northward flow across the Hebrides (Supplementary Figure 25). In other words, basin-scale circulation through the influence of SPG on NAC pathways not only influences where blue whiting spawn, but also how eggs and larvae are transported and nourished, with potential consequences on yearclass strength. These basin-scale states, and their implications for NAC pathways, the spatial distribution of blue whiting spawning and the dispersal patterns experienced by eggs and larvae across the Rockall region, are schematically illustrated in Figure 7.

Transport and current velocity through the Ellett Line exhibit only a weak covariation with the WSC index (Supplementary Figures 6-S7, S17), which likely reflects the fact that the WSC index is defined over a relatively small region which is located further south compared to the Ellett Line latitude, and therefore integrates wind forcing over a somewhat different water masses than those sampled by the section.

#### 4.4 Implications for stock structure

Evidence from stock structure studies suggests that blue whiting in the Northeast Atlantic is probably not a single homogeneous stock but a metapopulation composed of at least two semi-distinct components, northern and southern, linked by partial migration (Lee et al., 2025). Their review indicates that both migratory and resident subpopulations coexist, contributing to spatial complexity in blue whiting population structure (Lee et al., 2025). Genetic, otolith, parasite, and life-history markers point to relatively discrete northern and southern subpopulations, with intermediate mixing zones and locally resident groups (Mahe et al., 2016). Early Lagrangian modelling of blue whiting larvae identified a separation line around Porcupine Bank (53-54.5° N) between northward- and southward-drifting larvae, consistent with the evidence of two spawning stocks, and a transition zone Northeast of the bank where stock mixing occurs (Bartsch and Coombs, 1997; Skogen et al., 1999). The position of this dividing line shifted by up to 200 km among years, indicating interannual mixing between the two stock components (Skogen et al., 1999).



Empirical observations of blue whiting eggs and larvae further support Porcupine Bank as a critical stock boundary zone: under moderate wind conditions, an anticyclonic Taylor column over Porcupine Bank retains larvae locally, sustaining a self-recruiting resident population, whereas strong storms can disrupt this retention and flush larvae southward (Kloppmann et al., 2001). Thus, Porcupine Bank emerges as both a retention area supporting a local subpopulation and a mixing ground where northern and southern subpopulations can exchange genes (Lee et al., 2025). High retention associated with the Taylor column circulation over Porcupine Bank was also reported by Laiz et al. (2025), who showed that during the exceptional recruitment year of 2020, a persistent anticyclonic structure driven by weak wind mixing enhanced local retention and phytoplankton accumulation, thereby creating favorable trophic conditions for larval survival (Laiz et al., 2025).

Our ABM results resonate with the partial-migration hypothesis. Simulated larvae released in the Hebrides region are transported largely northward along the slope current, consistent with a migratory stock component that contributes to the northern subpopulation. In contrast, agents released from Porcupine Bank show higher local retention, characteristic of a resident group, with occasional southward drift in some years indicating connectivity with more southerly populations. Although blue whiting in the Northeast Atlantic is currently assessed as a single stock, the spatial heterogeneity in early life drift pathways highlights the need for spatially explicit management approaches and data types that

account for multiple stock components and their connectivity patterns (Lee et al., 2025).

#### 4.5 Study limitations and future directions

Our study highlights the role of regional circulation and transport in driving the survival of blue whiting early life stages, but several limitations should be acknowledged. First, we assume a constant share of egg production among all spawning areas specified in the ABM, even though spawning distribution of adults shifts with ocean-climate conditions (i.e., SPG state) (Hátún et al., 2009b; Miesner and Payne, 2018). For instance, Porcupine Bank and the Hebrides typically contribute a larger fraction of spawning than Rockall Plateau under strong SPG conditions (Hátún et al., 2009b). Moreover, spawning time differs by location: Porcupine Bank spawning peaks around March, whereas peak spawning in the northern Rockall Trough and Hebrides occurs later in spring (April-May) (Kloppmann et al., 2001; Pointin and Payne, 2014; Miesner and Payne, 2018; Miesner et al., 2022; ICES, 2022, 2024). Future Lagrangian simulations should incorporate spatially and temporally varying egg release (weighted by area-specific spawning distribution and time) to better reflect these dynamics. Second, our recruit per spawner index ( $\ln R/SSB$ ) is aggregated at the whole stock level, limiting our ability to attribute high or low recruit per spawner to specific sub-areas. Because the stock is assessed as a single unit (ICES, 2024), contributions of each of the spawning areas to yearclass success,

which are presently unknown, is combined into the overall index, complicating direct validation of area-specific dispersal patterns. New studies on characteristics of survivors, potentially using otolith micro-structure and micro-chemistry or genetic methods, could help determine which areas produce most survivors in different years and levels of connectivity among various spawning and nursery areas (Huyer et al., 2014; Wright et al., 2024; Lee et al., 2025). Third, the ABM treats larvae as passive drifters and does not include mortality, growth, predation, or food availability, so all agents are considered to have equal survival probability throughout the simulation. This is a simplification, as early life stages are highly sensitive to environmental conditions and characterized by high mortality (Bailey and Heath, 2001). Recruitment success depends not only on transport pathways but also on environmental processes: prolonged retention in nutrient-rich areas can enhance prey availability and larval survival (Laiz et al., 2025). Coupling drift trajectories with larval growth in relation to temperature, salinity, and food availability, and linking growth or body size to survival probability, could improve the accuracy of recruitment predictions based on ABM approaches and deepen the mechanistic understanding of blue whiting early life dynamics (e.g., Peck et al., 2006; Peck and Daewel, 2007; Peck and Hufnagl, 2012).

Our simulations use an oceanographic data product which does not explicitly include a vertical velocity component, which could represent the impacts of upwelling and other topographically-steered flows on larval vertical distribution. Such processes could locally lift larvae into faster surface flows, particularly along the steep slope in Rockall Trough and adjacent shelf break, thereby modifying the dispersal pathways, and potentially extending northward displacement (Mohn et al., 2023). We partly explore this limitation by running sensitivity tests on the simulated vertical behavior, constraining particles either to the surface layer (0–10 m) or to a deep layer (~350 m), and we compare these results with the simulated vertical behavior configuration. These sensitivity analyses reveal only modest changes in the drift patterns (Supplementary Figure 26–S27). In most spawning areas, surface runs show equal or slightly greater displacement, especially eastwards, and weaker retention, but the relative transport patterns observed across spawning areas and the qualitative contrast between the high- and low-recruit-per-spawner years is preserved. This suggests that, within the range of plausible vertical distributions we test, our main conclusions about spatial patterns of transport and their links to recruitment are robust, although future work using products with explicit vertical velocities would help to clarify the role of upwelling-driven and other vertical motions.

## 5 Conclusions

Our study provides a mechanistic interpretation of a recently detected relationship between wind stress curl and blue whiting recruitment by linking regional transport indices across the Ellett Line with high-resolution particle-tracking simulations. We find that strong northward transport along the Hebrides-Rockall Trough and large local retention over Porcupine Bank emerge as primary

drivers of early survival. This highlights the dual importance of dispersal and retention pathways: in years of high recruit per spawner, a strong SPG intensifies the NAC's poleward flow along the shelf edge, delivering eggs and larvae into cooler, nutrient-rich subpolar waters and ensuring effective drift toward northern nursery areas, whereas a weakened SPG tends to diminish this inflow and shift spawning offshore, where larvae may recirculate in less favorable conditions. Stable Taylor-column circulation over Porcupine Bank can promote larval survival by enhancing local retention, especially when associated with plankton blooms. By contrast, low-recruit-per-spawner years exhibit weaker shelf-break currents, more meandering trajectories, and a modest southward drift from Porcupine Bank, potentially limiting larval exposure to productive habitats. These findings suggest that shifts in the SPG-NAC system modulate recruitment success by altering retention/dispersal processes that influence survival probability, e.g., via exposure to food supplies. Incorporating spatially explicit spawning distributions and environment-dependent larval growth and survival rates in future ABM models will further improve our understanding of the mechanisms driving blue whiting recruitment success. Such advances will support more adaptive, ecosystem-based management of this ecologically and economically important species.

## Data availability statement

The raw data supporting the conclusions of this article will be made available by the authors, without undue reservation.

## Author contributions

CC: Conceptualization, Methodology, Visualization, Data curation, Investigation, Writing – review & editing, Writing – original draft, Formal analysis. HH: Supervision, Writing – review & editing, Funding acquisition, Conceptualization. JJ: Funding acquisition, Writing – review & editing, Supervision, Conceptualization. AV: Conceptualization, Funding acquisition, Writing – review & editing, Supervision. FH: Writing – review & editing, Supervision. JM: Methodology, Writing – review & editing. SA: Writing – review & editing, Methodology. FR: Writing – review & editing, Methodology. BM: Conceptualization, Project administration, Supervision, Writing – review & editing, Writing – original draft, Funding acquisition.

## Funding

The author(s) declared that financial support was received for this work and/or its publication. This work is part of the BlueOcean project, supported by the Research Council Faroe Islands (Granskingarráðið) through the MARiNAO (Marine research in

the North Atlantic Ocean; project 8013) program. This study has been conducted using E.U. Copernicus Marine Service Information (DOI 10.48670/moi-00021).

## Conflict of interest

Authors FH, JM, and SA were employed by company DHI A/S.

The remaining author(s) declared that this work was conducted in the absence of any commercial or financial relationships that could be construed as a potential conflict of interest.

## Generative AI statement

The author(s) declared that generative AI was used in the creation of this manuscript. OpenAI's ChatGPT was used for code troubleshooting and text editing of initial draft prepared by the co-authors.

Any alternative text (alt text) provided alongside figures in this article has been generated by Frontiers with the support of artificial

intelligence and reasonable efforts have been made to ensure accuracy, including review by the authors wherever possible. If you identify any issues, please contact us.

## Publisher's note

All claims expressed in this article are solely those of the authors and do not necessarily represent those of their affiliated organizations, or those of the publisher, the editors and the reviewers. Any product that may be evaluated in this article, or claim that may be made by its manufacturer, is not guaranteed or endorsed by the publisher.

## Supplementary material

The Supplementary Material for this article can be found online at: <https://www.frontiersin.org/articles/10.3389/fmars.2026.1764145/full#supplementary-material>

## References

- Ådlandsvik, B., Coombs, S., Sundby, S., and Temple, G. (2001). Buoyancy and vertical distribution of eggs and larvae of blue whiting (*Micromesistius poutassou*): observations and modelling. *Fish Res.* 50, 59–72. doi: 10.1016/S0165-7836(00)00242-3
- Akaike, H. (1973). "Information theory and an extension of the maximum likelihood principle," in *Second international symposium on information theory*. Eds. B. N. Petrov and F. Csaki (Akademiai Kiado, Budapest, Hungary), 267–281.
- Årthun, M., Brakstad, A., Dörr, J., Johnson, H. L., Mans, C., Semper, S., et al. (2025). Atlantification drives recent strengthening of the Arctic overturning circulation. *Sci. Adv.* 11, eadu1794. doi: 10.1126/sciadv.adu1794
- (2022). *Esri. ArcGIS pro (version 3.0.0)* (Redlands, CA: Environmental Systems Research Institute).
- Bachiller, E., Skaret, G., Nøttestad, L., and Slotte, A. (2016). Feeding ecology of northeast atlantic mackerel, norwegian spring-spawning herring and blue whiting in the norwegian sea. *PLoS One* 11, e0149238. doi: 10.1371/journal.pone.0149238
- Bailey, M. C., and Heath, M. R. (2001). Spatial variability in the growth rate of blue whiting (*Micromesistius poutassou*) larvae at the shelf edge west of the UK. *Fish Res.* 50, 73–87. doi: 10.1016/S0165-7836(00)00243-5
- Bartsch, J., and Coombs, S. (1997). A numerical model of the dispersion of blue whiting larvae, *Micromesistius poutassou* (Risso), in the eastern North Atlantic. *Fish Oceanogr.* 6, 141–154. doi: 10.1046/j.1365-2419.1997.00036.x
- Bergmeir, C., Hyndman, R. J., and Koo, B. (2018). A note on the validity of cross-validation for evaluating autoregressive time series prediction. *Comput. Stat. Data Anal.* 120, 70–83. doi: 10.1016/j.csda.2017.11.003
- Brooks, M. E., Kristensen, K., van Benthem, K. J., Magnusson, A., Berg, C. W., Nielsen, A., et al. (2017). glmmTMB balances speed and flexibility among packages for zero-inflated generalized linear mixed modeling. *R J.* 9, 378–400. doi: 10.32614/RJ-2017-066
- Brophy, D., and King, P. A. (2007). Larval otolith growth histories show evidence of stock structure in Northeast Atlantic blue whiting (*Micromesistius poutassou*). *ICES J. Mar. Sci.* 64, 1136–1144. doi: 10.1093/icesjms/fsm080
- Burnham, K. P., and Anderson, D. R. (2002). *Model selection and multimodel inference: A practical information-theoretic approach. 2nd edn* (New York, NY: Springer-Verlag).
- Burnham, K. P., Anderson, D. R., and Huyvaert, K. P. (2011). AIC model selection and multimodel inference in behavioral ecology: some background, observations, and comparisons. *Behav. Ecol. Sociobiol.* 65, 23–35. doi: 10.1007/s00265-010-1029-6
- Cappelli, C. (2025). BlueWhiting\_Transport. Available online at: [https://github.com/costanzacappelli/BlueWhiting\\_Transport](https://github.com/costanzacappelli/BlueWhiting_Transport) (Accessed 8 December 2025).
- Cappelli, C., Hátún, H., Jacobsen, J. A., Visser, A. W., Nielsen, A., Berg, C. W., et al. (2025). Ocean-climate conditions one year prior to spawning drive recruitment success of blue whiting. *ICES J. Mar. Sci.* 82, fsaf102. doi: 10.1093/icesjms/fsaf102
- Chafik, L., Nilsen, J. E. Ø., Dangendorf, S., Reverdin, G., and Frederikse, T. (2019). North atlantic ocean circulation and decadal sea level change during the altimetry era. *Sci. Rep.* 9, 1041. doi: 10.1038/s41598-018-37603-6
- Chafik, L., Nilsson, J., Rossby, T., and Kondetharayil Soman, A. (2023). The Faroe-Shetland Channel jet: Structure, variability, and driving mechanisms. *J. Geophys. Res. Oceans* 128, e2022JC019083. doi: 10.1029/2022JC019083
- Coombs, S. H., and Hiby, A. R. (1979). The development of the eggs and early larvae of blue whiting, *Micromesistius poutassou* and the effect of temperature on development. *J. Fish Biol.* 14, 111–123. doi: 10.1111/j.1095-8649.1979.tb03500.x
- Copernicus Marine Service (2021). Global ocean physics reanalysis (GLORYS12V1) [Product ID: GLOBAL\_MULTIYEAR\_PHY\_001\_030] (E.U. Copernicus Marine Service (CMEMS)). Available online at: <https://data.marine.copernicus.eu>. doi: 10.48670/moi-00021
- Cresci, A., Sandvik, A. D., Sævik, P. N., Mykssvoll, M. S., Albreten, J., Durif, C. M. F., et al. (2025). Orientation and swimming behavior of saithe (*Pollachius virens*) larvae increases the chance of recruitment to nursery areas. *Fish Oceanogr.* doi: 10.1111/fog.70008
- DHI (2016a). *MIKE 3 flow model FM. ECO lab/oil spill module. User guide* (Hørsholm, Denmark: DHI).
- DHI (2016b). *MIKE 3 flow model FM. Hydrodynamic module. User guide* (Hørsholm, Denmark: DHI).
- Eden, C., and Willebrand, J. (2001). Mechanism of interannual to decadal variability of the north atlantic circulation. *J. Clim.* 14, 2266–2280. doi: 10.1175/1520-0442(2001)014<2266:MOITDV>2.0.CO;2
- Gary, S. F., Cunningham, S. A., Johnson, C., Houpt, L., Holliday, N. P., Behrens, E., et al. (2018). Seasonal cycles of oceanic transports in the eastern subpolar north atlantic. *J. Geophys. Res. Oceans* 123, 1471–1484. doi: 10.1002/2017JC013350
- Häkkinen, S., and Rhines, P. B. (2004). Decline of subpolar north atlantic circulation during the 1990s. *Science* 304, 555–559. doi: 10.1126/science.1094917
- Häkkinen, S., Rhines, P. B., and Worthen, D. L. (2011). Warm and saline events embedded in the meridional circulation of the northern North Atlantic. *J. Geophys. Res.* 116, C03006. doi: 10.1029/2010JC006275
- Hátún, H., and Chafik, L. (2018). On the recent ambiguity of the North Atlantic subpolar gyre index. *J. Geophys. Res. Oceans* 123, 5072–5076. doi: 10.1029/2018JC014101

- Hátún, H., Larsen, K. M. H., Káradóttir Eliassen, S., and Mathis, M. (2021). "Major nutrient fronts in the Northeastern Atlantic: From the subpolar gyre to adjacent shelves," in *Chemical oceanography of frontal zones. The handbook of environmental chemistry*, vol 116. Ed. I. M. Belkin (Springer, Berlin, Heidelberg), 97–141. doi: 10.1007/978-2021\_794
- Hátún, H., Payne, M. R., Beaugrand, G., Reid, P. C., Sandø, A. B., Drange, H., et al. (2009a). Large bio-geographical shifts in the north-eastern Atlantic Ocean: From the subpolar gyre, via plankton, to blue whiting and pilot whales. *Prog. Oceanogr* 80, 149–162. doi: 10.1016/j.pocean.2009.03.001
- Hátún, H., Payne, M. R., and Jacobsen, J. A. (2009b). The North Atlantic subpolar gyre regulates the spawning distribution of blue whiting (*Micromesistius poutassou*). *Can. J. Fish Aquat Sci.* 66, 759–770. doi: 10.1139/F09-037
- Hátún, H., Sandø, A. B., Drange, H., Hansen, B., and Valdimarsson, H. (2005). Influence of the atlantic subpolar gyre on the thermohaline circulation. *Science* 309, 1841–1844. doi: 10.1126/science.1114777
- Henriksen, O., Christensen, A., Jónasdóttir, S., MacKenzie, B. R., Nielsen, K. E., Mosegård, H., et al. (2018). Oceanographic flow regime and fish recruitment: reversed circulation in the North Sea coincides with unusually strong sandeel recruitment. *Mar. Ecol. Prog. Ser.* 607, 187–205. doi: 10.3354/meps12786
- Hillgruber, N., and Klöppmann, M. (1999). Distribution and feeding of blue whiting (*Micromesistius poutassou*) larvae in relation to different water masses in the Porcupine Bank area, west of Ireland. *Mar. Ecol. Prog. Ser.* 187, 213–225. doi: 10.3354/meps187213
- Holliday, N. P. (2003). Air–sea interaction and circulation changes in the northeast Atlantic. *J. Geophys Res.* 108, 3259. doi: 10.1029/2002JC001344
- Holliday, N. P., Bersch, M., Bex, B., Chafik, L., Cunningham, S., Florindo-López, C., et al. (2020). Ocean circulation causes the largest freshening event for 120 years in eastern subpolar North Atlantic. *Nat. Commun.* 11, 585. doi: 10.1038/s41467-020-14474-y
- Holliday, N. P., Hughes, S. L., Bacon, S., Szczepanska-Möller, A., Hansen, B., Lavín, A., et al. (2008). Reversal of the 1960s to 1990s freshening trend in the northeast North Atlantic and Nordic Seas. *Geophys Res. Lett.* 35, L03614. doi: 10.1029/2007GL032675
- Holliday, N. P., Pollard, R. T., Read, J. F., and Leach, H. (2000). Water mass properties and fluxes in the Rockall Trough 1975–1998. *Deep-Sea Res. I* 47, 1303–1332. doi: 10.1016/S0967-0637(99)00109-0
- Houpert, L., Cunningham, S., Fraser, N., Johnson, C., Holliday, N. P., Jones, S., et al. (2020). Observed variability of the north atlantic current in the rockall trough from 4 years of mooring measurements. *J. Geophys Res. Oceans* 125, e2020JC016403. doi: 10.1029/2020JC016403
- Huang, J., Pickart, R. S., Chen, Z., and Huang, R. X. (2023). Role of air–sea heat flux on the transformation of Atlantic Water encircling the Nordic Seas. *Nat. Commun.* 14, 141. doi: 10.1038/s41467-023-35889-3
- Huwer, B., Hinrichsen, H. H., Böttcher, U., Voss, R., and Köster, F. W. (2014). Characteristics of juvenile survivors reveal spatio-temporal differences in early life stage survival of Baltic cod. *Mar. Ecol. Prog. Ser.* 511, 165–180. doi: 10.3354/meps10875
- ICES (2022). *Stock Annex: Blue whiting (Micromesistius poutassou) in subareas 1–9, 12, and 14 (Northeast Atlantic and adjacent waters)* (ICES Stock Annex), 46pp. doi: 10.17895/ices.pub.21105808
- ICES (2024). *Working group on widely distributed stocks (WGWIDE)* Vol. 6 (ICES Scientific Reports), 913 pp. doi: 10.17895/ices.pub.26993227
- Jacox, M. G., Edwards, C. A., Hazen, E. L., and Bograd, S. J. (2018). Coastal upwelling revisited: ekman, bakun, and improved upwelling indices for the U.S. West coast. *J. Geophys Res. Oceans* 123, 7332–7350. doi: 10.1029/2018JC014187
- Jansen, T., Hansen, F. T., and Bardason, B. (2021). Larval drift dynamics, thermal conditions and the shift in juvenile capelin distribution and recruitment success around Iceland and East Greenland. *Fish Res.* 236, 105845. doi: 10.1016/j.fishres.2020.105845
- Johnson, C., Inall, M., and Häkkinen, S. (2013). Declining nutrient concentrations in the northeast Atlantic as a result of a weakening Subpolar Gyre. *Deep Sea Res. Part Oceanogr Res. Pap* 82, 95–107. doi: 10.1016/j.dsr.2013.08.007
- Klöppmann, M., Mohn, C., and Bartsch, J. (2001). The distribution of blue whiting eggs and larvae on Porcupine Bank in relation to hydrography and currents. *Fish Res.* 50, 89–109. doi: 10.1016/S0165-7836(00)00244-7
- Laiz, I., Chowdhury, M., González-Nuevo, G., Velasco, F., and Baldó, F. (2025). Unravelling the environmental drivers of blue whiting recruitment: 20 years of observations. *Front. Mar. Sci.* 12. doi: 10.3389/fmars.2025.1535712
- Lee, B., Ólafsdóttir, A. H., Post, S., Jacobsen, J. A., Hoines, Å., Gonçalves, P., et al. (2025). Unravelling the stock structure of blue whiting in the Northeast Atlantic: navigating contradictions towards resolution. *Rev. Fish Biol. Fish.* doi: 10.1007/s11160-025-09976-1
- Lellouche, J.-M., Greiner, E., Bourdallé-Badie, R., Garric, G., Melet, A., Drévillon, M., et al. (2021). The copernicus global 1/12° Oceanic and sea ice GLORYS12 reanalysis. *Front. Earth Sci.* 9. doi: 10.3389/feart.2021.698876
- Magnusson, A., Skaug, H. J., Nielsen, A., et al. (2019). *Generalized linear mixed models using Template Model Builder*.
- Mahe, K., Oudard, C., Mille, T., et al. (2016). Identifying blue whiting (*Micromesistius poutassou*) stock structure in the northeast Atlantic by otolith shape analysis. *Can. J. Fish Aquat Sci.* 73, 1363–1371. doi: 10.1139/cjfas-2015-0332
- Miesner, A. K., Brune, S., Pieper, P., et al. (2022). Exploring the potential of forecasting fish distributions in the north east atlantic with a dynamic earth system model, exemplified by the suitable spawning habitat of blue whiting. *Front. Mar. Sci.* 8. doi: 10.3389/fmars.2021.777427
- Miesner, A. K., and Payne, M. R. (2018). Oceanographic variability shapes the spawning distribution of blue whiting (*Micromesistius poutassou*). *Fish Oceanogr* 27, 623–638. doi: 10.1111/fog.12382
- Mohn, C., Hansen, J. L. S., Carreiro-Silva, M., et al. (2023). Tidal to decadal scale hydrodynamics at two contrasting cold-water coral sites in the Northeast Atlantic. *Prog. Oceanogr* 214, 103031. doi: 10.1016/j.pocean.2023.103031
- National Oceanography Centre About the Ellett Array (Ellett Array project). Available online at: <https://projects.noc.ac.uk/ellett-array/about> (Accessed 3 September 2024).
- Payne, M. R., Egan, A., Fässler, S. M. M., et al. (2012). The rise and fall of the NE Atlantic blue whiting (*Micromesistius poutassou*). *Mar. Biol. Res.* 8, 475–487. doi: 10.1080/17451000.2011.639778
- Peck, M. A., Buckley, L. J., and Bengtson, D. A. (2006). Effects of temperature and body size on the swimming speed of larval and juvenile Atlantic cod (*Gadus morhua*): Implications for individual-based modelling. *Environ. Biol. Fishes* 75, 419–442. doi: 10.1007/s10641-006-0031-3
- Peck, M. A., and Daewel, U. (2007). Physiologically based limits to food consumption, and individual-based modelling of foraging and growth of larval fishes. *Mar. Ecol. Prog. Ser.* 347, 171–183. doi: 10.3354/meps06976
- Peck, M. A., and Hufnagl, M. (2012). Can IBMs tell us why most larvae die in the sea? Model sensitivities and scenarios reveal research needs. *J. Mar. Syst.* 93, 77–93. doi: 10.1016/j.jmarsys.2011.08.005
- Pereira Gabellini, A., Mariani, P., and Christensen, A. (2023). Population connectivity and dynamics in early-life stages of Atlantic fish communities. *Front. Mar. Sci.* 10. doi: 10.3389/fmars.2023.1141726
- Pointin, F., and Payne, M. R. (2014). A resolution to the blue whiting (*Micromesistius poutassou*) population paradox? *PLoS One* 9, e106237. doi: 10.1371/journal.pone.0106237
- Post, S., Jónasdóttir, S. H., Andreassen, H., et al. (2021). Blue whiting *Micromesistius poutassou* diel feeding behaviour in the Irminger Sea. *Mar. Ecol. Prog. Ser.* 678, 1–16. doi: 10.3354/meps13918
- R Core Team (2022). *R: A language and environment for statistical computing* (Vienna, Austria: R Foundation for Statistical Computing).
- Romagnoni, G., Kville, KØ, Dagestad, K.-F., et al. (2020). Influence of larval transport and temperature on recruitment dynamics of North Sea cod (*Gadus morhua*) across spatial scales of observation. *Fish Oceanogr* 29, 324–339. doi: 10.1111/fog.12474
- Roux, M.-J., and Pedreschi, D. (2024). ICES framework for ecosystem-informed science and advice (FEISA). *ICES Coop Res. Rep.* 359, 39.
- Sinclair, M. (1988). *Marine populations: an essay on population regulation and speciation* (Washington Sea Grant Program: Distributed by University of Washington Press).
- Skogen, M. D., Monstad, T., and Svendsen, E. (1999). A possible separation between a northern and a southern stock of the northeast Atlantic blue whiting. *Fish Res.* 41, 119–131. doi: 10.1016/S0165-7836(99)00019-3
- Thygesen, U. H., Albertsen, C. M., Berg, C. W., et al. (2017). Validation of ecological state space models using the Laplace approximation. *Environ. Ecol. Stat.* 24, 317–339. doi: 10.1007/s10651-017-0372-4
- Trenkel, V. M., Huse, G., MacKenzie, B. R., et al. (2014). Comparative ecology of widely distributed pelagic fish species in the North Atlantic: Implications for modelling climate and fisheries impacts. *Prog. Oceanogr* 129, 219–243. doi: 10.1016/j.pocean.2014.04.030
- Tyldesley, E., Banas, N. S., Diack, G., et al. (2024). Patterns of declining zooplankton energy in the northeast Atlantic as an indicator for marine survival of Atlantic salmon. *ICES J. Mar. Sci.* 81, 1164–1184. doi: 10.1093/icesjms/fsae077
- Ullgren, J. E., and White, M. (2012). Observations of mesoscale variability in the Rockall Trough. *Deep Sea Res. Part I Oceanogr Res. Pap* 64, 1–8. doi: 10.1016/j.dsr.2012.01.015
- van Aken, H. M. (2001). The hydrography of the mid-latitude Northeast Atlantic Ocean — Part III: the subtended thermocline water mass. *Deep Sea Res. Part I Oceanogr Res. Pap* 48, 237–267. doi: 10.1016/S0967-0637(00)00059-5
- Verezemskaya, P., Barnier, B., Gulev, S. K., et al. (2021). Assessing eddying (1/12°) ocean reanalysis GLORYS12 using the 14-yr instrumental record from 59.5°N section in the atlantic. *J. Geophys Res. Oceans* 126, e2020JC016317. doi: 10.1029/2020JC016317
- Visser, A. W. (1997). Using random walk models to simulate the vertical distribution of particles in a turbulent water column. *Mar. Ecol. Prog. Ser.* 158, 275–281. doi: 10.3354/meps158275
- Was, A., Gosling, E., McCrann, K., et al. (2008). Evidence for population structuring of blue whiting (*Micromesistius poutassou*) in the Northeast Atlantic. *ICES J. Mar. Sci.* 65, 216–225. doi: 10.1093/icesjms/fsm187
- Williams, R. G., and Follows, M. J. (2003). "Physical transport of nutrients and the maintenance of biological production," in *Ocean biogeochemistry*. Ed. M. J. R. Fasham (Springer Berlin Heidelberg, Berlin, Heidelberg), 19–51. doi: 10.1007/978-3-642-55844-3\_3
- Wright, P. J., Dobby, H., and Fox, C. (2024). "Northwest European Shelf cod stocks; North Sea, West of Scotland, Irish Sea and Celtic Sea," in *Biology and ecology of atlantic cod*. Eds. N. Kulatska, D. Howell, P. J. Wright and I. G. Jónsdóttir (CRC Press, Boca Raton, FL), 136–173. doi: 10.1201/9781003120872-7